iScience

CellPress
OPEN ACCESS

Article

Antagonism among DUX family members evolved from an ancestral toxic single homeodomain protein

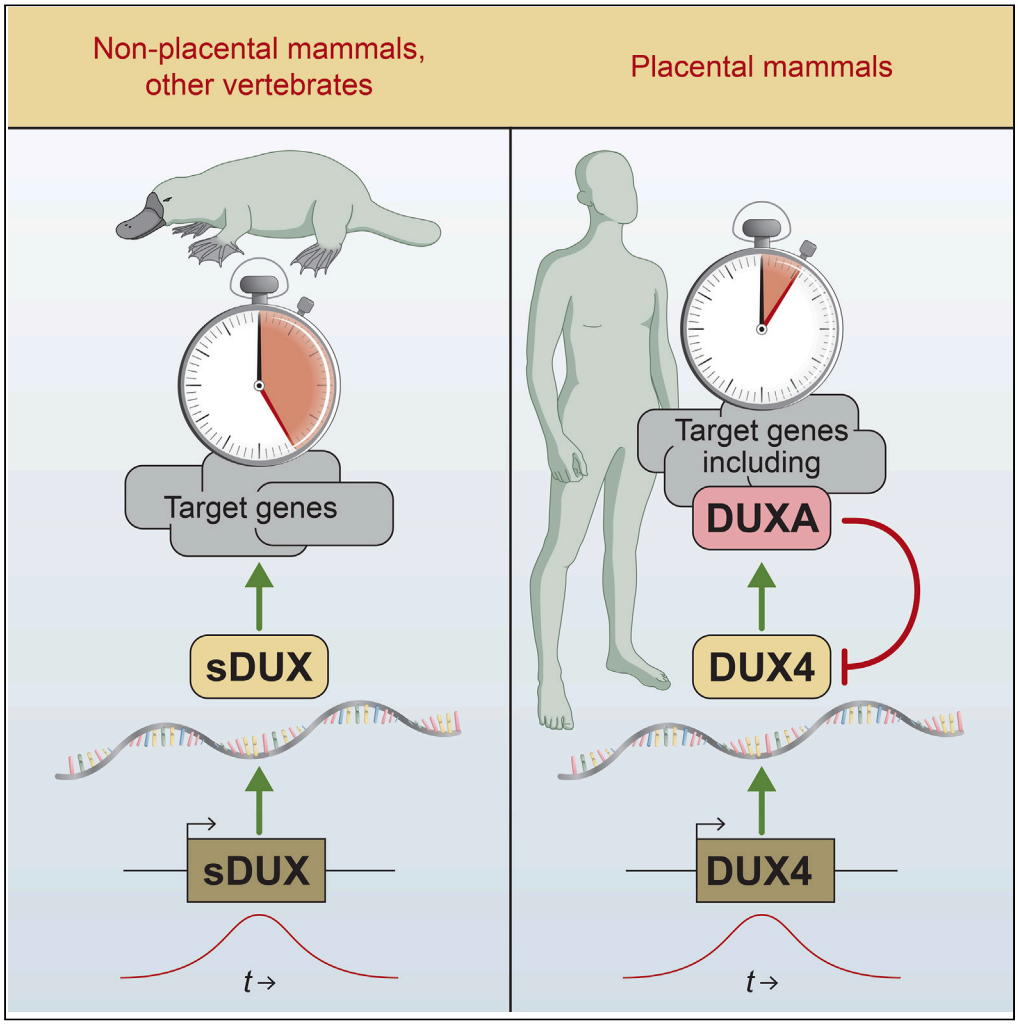

Darko Bosnakovski, Erik A. Toso, Elizabeth T. Ener, ..., Johnny Kim, Hideki Aihara, Michael Kyba

kyba@umn.edu

Highlights

Platypus sDUX is toxic and inhibits myogenic differentiation

DUXA targets overlap substantially with those of DUX4

DUXA fused to a synthetic transactivation domain acquires DUX4-like toxicity

DUXA behaves as a competitive inhibitor of DUX4

Bosnakovski et al., iScience 26, 107823
October 20, 2023
https://doi.org/10.1016/j.isci.2023.107823

iScience

CellPress
OPEN ACCESS

Article

Antagonism among DUX family members evolved from an ancestral toxic single homeodomain protein

Darko Bosnakovski,[1,2] Erik A. Toso,[1,2] Elizabeth T. Ener,[1,2] Micah D. Gearhart,[3] Lulu Yin,[4] Felipe F. Lüttmann,[5] Alessandro Magli,[6] Ke Shi,[4] Johnny Kim,[5,7] Hideki Aihara,[4] and Michael Kyba[1,2,8,*]

SUMMARY

Double homeobox (DUX) genes are unique to eutherian mammals, expressed transiently during zygotic genome activation (ZGA) and involved in facioscapulohumeral muscular dystrophy (FSHD) and cancer when misexpressed. We evaluate the 3 human DUX genes and the ancestral single homeobox gene sDUX from the non-eutherian mammal, platypus, and find that DUX4 cytotoxicity is not shared with DUXA or DUXB, but surprisingly is shared with platypus sDUX, which binds DNA as a homodimer and activates numerous ZGA genes and long terminal repeat (LTR) elements. DUXA, although transcriptionally inactive, has DNA binding overlap with DUX4, and DUXA-VP64 activates DUX4 targets and is cytotoxic. DUXA competition antagonizes the activity of DUX4 on its target genes, including in FSHD patient cells. Since DUXA is a DUX4 target gene, this competition potentiates feedback inhibition, constraining the window of DUX4 activity. The DUX gene family therefore comprises antagonistic members of opposing function, with implications for their roles in ZGA, FSHD, and cancer.

INTRODUCTION

The double homeobox (DUX) gene family is unique to eutherian mammals.[1] Although some homeodomain (HD)-containing transcription factors have a second DNA-binding domain of a different type, the presence of two HDs in tandem does not occur elsewhere in the tree of life. The DUX gene family is derived from an ancestral single homeobox gene, named *sDUX*, present in fish, lizards, birds, and non-eutherian mammals, via tandem duplication of the *sDUX* single homeobox.[2] This new DUX gene then expanded, diverging within the ancestral placental mammal genome into three clades: DUXA, DUXB, and DUXC, with DUXC genes uniquely expanding massively into long tandem arrays, while DUXA and DUXB remained present at low or single copy[2] (Figure 1A). There has been significant sequence diversion within each HD, demonstrated by the fact that sequence dendrograms do not cluster HD1 sequences from DUXA, B, and C together, nor those of HD2, but rather, each HD of each DUX clade is rooted deeply, each practically as distant from the sDUX HD as the others (Figure 1B). In humans, the DUXC representative is named *DUX4*,[3] and its tandem arrays are subject to repeat-induced silencing.[4] If the array contracts to low copy numbers, the silencing becomes inefficient, leading, by way of leaky expression of *DUX4*,[5] to the disease, facioscapulohumeral muscular dystrophy (FSHD).[6] DUX4 is toxic to myoblasts and other cell types[7,8] and also impairs myoblast differentiation when expressed at low non-toxic levels.[8,9] Besides the HDs, DUXC family members share a conserved domain at the C terminus, which is not found in DUXA and DUXB family members.[1,2] The DUX4 C-terminal domain is an activation domain necessary for target gene expression,[10,11] is essential for cytotoxicity,[12] and confers transcriptional activation and pioneer activity to DUX4 by interacting with histone acetyltransferases (HATs) p300 and CBP to mediate histone H3 acetylation, chromatin opening, and transcription of target genes.[13] This C-terminal conservation is not found in various sDUX representatives, thus it is unclear whether sDUX is a transcriptional activator.

Both the mouse and human DUXC genes (*Dux* and *DUX4*) are briefly expressed in the cleavage stage embryo, at the 2- and 4-cell stage, respectively, where they activate a subset of genes expressed during zygotic genome activation (ZGA),[14,15] and so were proposed to be key inducers of ZGA.[16] However, because most species lack DUXC genes, because mouse *Dux* array knockouts (KOs) are viable,[17–19] because the majority of ZGA-associated genes are still expressed in the absence of *Dux*, because the rate of failure of KO embryos to develop to blastocyst *in vitro* is much higher than their rate of failure *in vivo*,[18] and because growth defects characterize a subset of *Dux* KO embryos, it has been

[1]Lillehei Heart Institute, University of Minnesota, Minneapolis, MN 55455, USA
[2]Department of Pediatrics, University of Minnesota, Minneapolis, MN 55455, USA
[3]Department of Genetics, Cell Biology and Development, University of Minnesota, Minneapolis, MN 55455, USA
[4]Department of Biochemistry, Molecular Biology, and Biophysics, University of Minnesota, Minneapolis, MN 55455, USA
[5]Max Planck Institute for Heart and Lung Research, Bad Nauheim, Germany
[6]Department of Cardiology, University of Minnesota, Minneapolis, MN 55455, USA
[7]The Center for Cardiovascular Regeneration and Immunology at TRON – Translational Oncology, Johannes Gutenberg-University Mainz, Mainz, Germany
[8]Lead contact
*Correspondence: kyba@umn.edu
https://doi.org/10.1016/j.isci.2023.107823

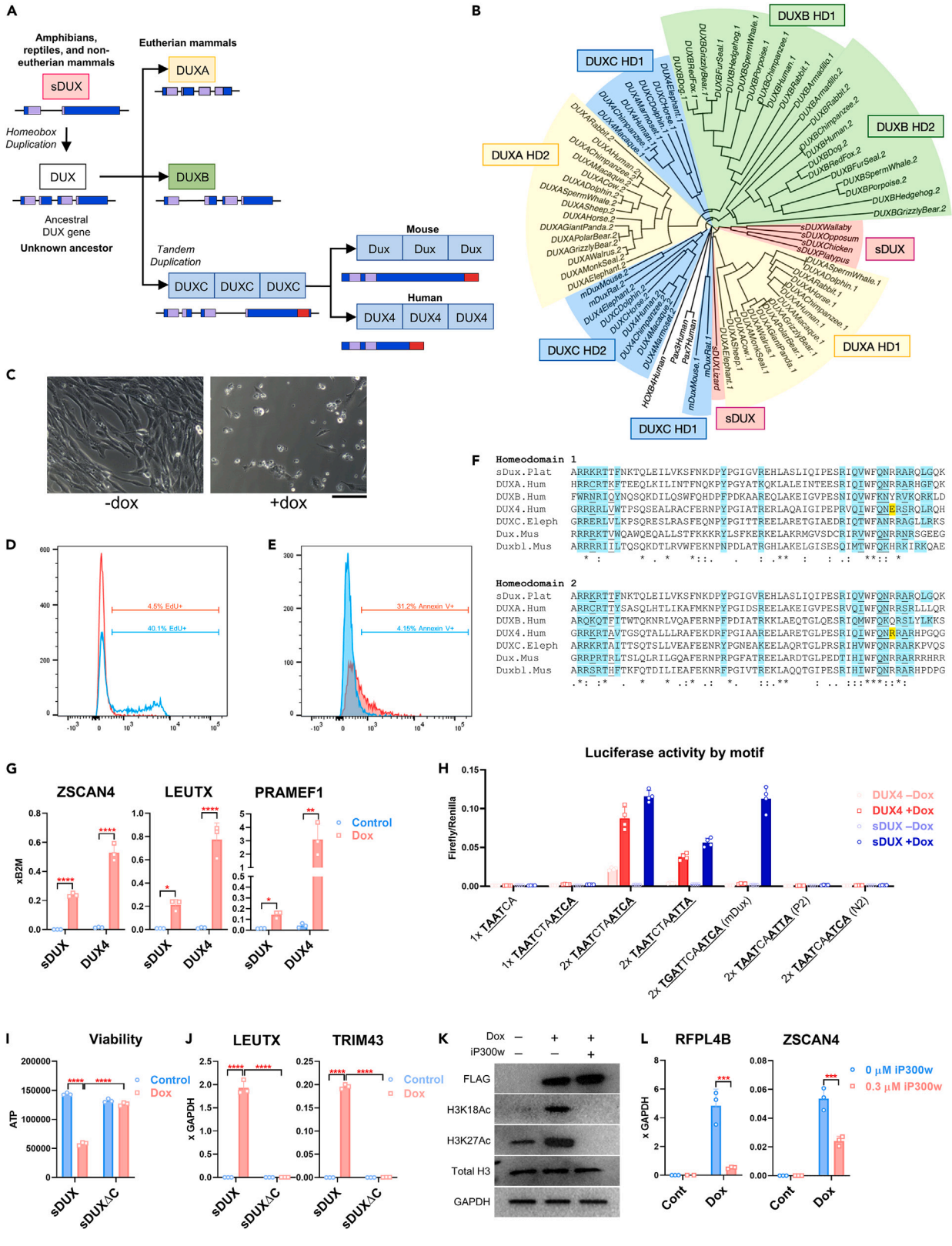
A
Amphibians, reptiles, and non-eutherian mammals
Eutherian mammals
sDUX
DUXA
Homeobox Duplication
DUX
DUXB
Ancestral DUX gene
Unknown ancestor
Tandem Duplication
DUXC DUXC DUXC
Mouse
Dux Dux Dux
Human
DUX4 DUX4 DUX4
B
DUXB HD1
DUXC HD1
DUXB HD2
DUXA HD2
sDUX
DUXC HD2
DUXA HD1
sDUX
C
-dox
+dox
D
4.5% EdU+
40.1% EdU+
E
31.2% Annexin V+
4.15% Annexin V+
F
Homeodomain 1
sDux.Plat ARRKRTTFNKTQLEILVKSFNKDPYPGIGVREHLASLIQIPESRIQVWFQNRRARQLGQK
DUXA.Hum HRRCRTKFTEEQLKILINTFNQKPYPGYATKQKLALEINTEESRIQIWFQNRRARNHGFQK
DUXB.Hum FWRNRIQYNQSQKDILQSWFQHDPFPDKAAREQLAKEIGVPESNIQVWFKNYRVKQRKLD
DUX4.Hum GRRRRLVWTPSQSEALRACFERNPYPGIATRERLAQAIGIPEPRVQIWFQNERSRQLRQH
DUXC.Eleph GRRERLVLKPSQRESLRASFEQNPYPGITTREELARETGIAEDRIQTWFANRRAGLLRKS
Dux.Mus RRRRKTVWQAWQEQALLSTFKKKRYLSFKEREKELAKRMGVSDCRIRVWFQNRRNRSGEEG
Duxbl.Mus ARRRRIILTQSQKDTLRVWFEKNPNPDLATRGHLAKELGISESQIMTWFQKHRKIRKQAE
Homeodomain 2
sDux.Plat ARRKRTTFNKTQLEILVKSFNKDPYPGIGVREHLASLIQIPESRIQVWFQNRRARQLGQK
DUXA.Hum ARRCRTTYSASQLHTLIKAFMKNPYPGIDSREELAKEIGVPESRVQIWFQNRRSRLLLQR
DUXB.Hum ARQKQTFITWTQKNRLVQAFERNPFPDIATRKKLAEQTGLQESRIQMWFQKQRSLYLKKS
DUX4.Hum GRRKRTAVTGSQTALLLRAFEKDRFPGIAAREELARETGLPESRIQIWFQNRRARHPGQG
DUXC.Eleph ARRKRTAITTSQTSLLVEAFEENRYPGNEAKEELAQRTGLPRSRIHVWFQNRRARKPVQS
Dux.Mus GRRPRTRLTSLQLRILGQAFERNPRPGFATREELARDTGLPEDTIHIWFQNRRARRHRR
Duxbl.Mus ARRSRTHFTKFQTDILIEAFEKNRFPGIVTREKLAQQTGIPESRIHIWFQNRRARHPDPG
G
ZSCAN4
LEUTX
PRAMEF1
xB2M
Control
Dox
sDUX
DUX4
H
Luciferase activity by motif
Firefly/Renilla
DUX4 –Dox
DUX4 +Dox
sDUX –Dox
sDUX +Dox
1x TAATCA
1x TAATCTAATCA
2x TAATCTAATCA
2x TAATCTAATTA
2x TGATTCAATCA (mDux)
2x TAATCAATTA (P2)
2x TAATCAATCA (N2)
I
Viability
ATP
Control
Dox
sDUX
sDUXΔC
J
LEUTX
TRIM43
x GAPDH
K
Dox
iP300w
FLAG
H3K18Ac
H3K27Ac
Total H3
GAPDH
L
RFPL4B
ZSCAN4
x GAPDH
0 μM iP300w
0.3 μM iP300w
Cont
Dox

Figure 1. Platypus sDUX displays functional overlap with DUX4

(A) Evolution of the DUX gene family from an ancestral single homeobox gene in the common ancestor to eutherian mammals.

(B) Sequence dendrogram of DUX homeodomains. DUX family members are shaded yellow (DUXA), green (DUXB), and blue (DUXC); and sDUX is shaded red.

(C) Morphology of LHCN-M2isDUX human myoblasts in the absence (left) or presence of 100 ng/mL dox for 4 days to induce sDUX (right). Scale bar, 100 μm.

(D) EdU incorporation in LHCN-M2isDUX human myoblasts after 6 h in the absence (blue) or presence (red) of 500 ng/mL dox to induce sDUX. X axis, counts; Y axis, fluorescence.

(E) Annexin V staining in LHCN-M2isDUX human myoblasts after 24 h in the absence (blue) or presence (red) of 500 ng/mL dox to induce sDUX. X axis, counts; Y axis, fluorescence.

(F) Sequence comparison of the sDUX homeodomain with HD1 and HD2 of the 3 human DUX family members, DUXC from elephant and mouse, and mouse DUXBL. Known or predicted DNA binding regions are highlighted in blue, and residues known or predicted to have specific nucleotide base contacts are underlined. Yellow shading indicates the E and R residues responsible for TAAT or TGAT specificities of DUX4 HD1 and HD2, resp. Asterisks indicate positions with a conserved residue, colons indicate conservation of strongly similar biochemical properties, periods indicate conservation between amino acids of weakly similar properties.

(G) Real time RTqPCR for *ZSCAN4*, *LEUTX*, and *PRAMEF1* in LHCN-M2iDUX4 parent and LHCN-M2-is DUX myoblasts induced with 200 ng/mL doxycycline for 14 h. Data are presented as mean ± SEM; *p < 0.05, ***p < 0.01**, ****p < 0.0001 by one-way ANOVA, n = 3.

(H) Luciferase assays in comparing activity of DUX4 and sDUX on different versions of the double homeodomain motif in 293T cells exposed to 500 ng/mL dox for 24 h. The core HD binding sites are underlined. DUX4 and DUX cores are separated by 3 nt while the PAX7 recognition motif cores are separated by 2 nt. Copy number of motifs indicated by 1x or 2x. Data are presented as mean ± SEM; n = 4.

(I) Viability assay for 293T cells after 48 h of expression (100 ng/mL dox) of full length sDUX vs. sDUXΔC, lacking the C-terminal 74 amino acids. Data are presented as mean ± SEM; n = 3.

(J) Real time RTqPCR for DUX4 target genes *LEUTX* and *TRIM43* after expression of sDUX or sDUXΔC in the same cells in panel I (500 ng/mL, 24 h). Data are presented as mean ± SEM; n = 3.

(K) Representative western blots with acetylation specific-antibodies in human myoblasts expressing sDUX and treated with the p300/CBP-specific HAT inhibitor, iP300w. LHCN-isDUX cells were induced with 200 ng/mL doxycycline and concurrently treated with 0.3 μM iP300w for 12 h.

(L) Real time RTqPCR for sDUX target genes *RFPL4B* and *ZSCAN4* in the presence or absence of iP300w on the cell presented in panel (K) Data are presented as mean ± SEM; n = 3.

proposed that this transient expression and downstream 4/8 cell target gene expression prime the embryo for later efficacious placentation rather than initiating ZGA *per se*.[18] In any case, the expression of DUXC family members is tightly restricted to early blastomere stages of embryogenesis, with a strong need for silencing in later somatic cells.

DUX genes have also been implicated in cancer, with one study suggesting that DUX4 expression leads to downregulation of major histocompatibility complex (MHC) proteins and thereby poor outcomes,[20] and another showing that amplification of murine *Duxbl* cooperates with p53 inactivation to drive rhabdomyosarcoma.[21] Interestingly, the latter study found that in human cells, *DUXA* was a strongly induced downstream target of DUX4 (*DUXB* was also induced at a lower level). This suggested the possibility of feedforward regulation within the family. Because DUX4 is virtually impossible to detect at the protein level in FSHD patient muscle biopsies, it was suggested that early transient DUX4 expression may set up a pathological program that persists long after a DUX4 burst.[22] Recent RNA sequencing (RNA-seq) data on cultured FSHD myoblasts revealed a population of *DUXA*+ cells that lacks *DUX4* expression, prompting a model in which DUXA takes over the induction of DUX4 target genes after a burst of DUX4 expression;[23] however, the transcriptional activity of DUXA is unknown. A mechanistic understanding of the role of the DUX family in development, FSHD, and cancer thus requires understanding the interplay between DUXA, B, and C and how their functions evolved from and relate to those of the ancestor, sDUX.

RESULTS

sDUX binds DUX motifs and is toxic to human myoblasts

To frame and root the function of the DUX family, we began by investigating sDUX from a species closely related to eutherian mammals, namely the monotreme *Ornithorhynchus anatinus* (platypus). Remarkably, doxycycline (dox)-inducible expression of platypus sDUX led to cell death of human myoblasts, in a manner very similar to that seen with DUX4 (Figure 1C). sDUX-expressing myoblasts ceased proliferating and underwent apoptosis as assessed by EdU (5-Ethynyl-2′-deoxyuridine) incorporation (Figure 1D) and annexin V staining (Figure 1E). Structural studies on the DUX4 HDs[24] have identified a critical residue (E vs. R) in helix 3 that specifies the TAAT vs. TGAT core preference (yellow residues in Figure 1F). DUX4 HD1, which bears E at this site, prefers TAAT, and HD2, which bears R, prefers TGAT (ATCA in the motif, since the HDs bind head-to-head), while both murine DUX HD1 and HD2 bear R and thus prefer TGAT (ATCA at the 3′ end of the motif). The sequence of the sDUX HD predicts a DNA-binding specificity similar to that of murine DUX. Despite this prediction, real time RTqPCR revealed that in human myoblasts, sDUX induced the canonical DUX4 target genes *ZSCAN4, LEUTX*, and *MBD3L2* (Figure 1G). To probe the sequence specificity of sDUX, we tested the ability of sDUX and DUX4 to transactivate from variations of double HD recognition motifs on luciferase expression plasmids bearing two copies of each motif upstream of a minimal promoter. While DUX4 clearly preferred the non-palindromic TAAT—ATCA motif (named N3 for non-palindromic with 3 nt spacing), sDUX was able to drive luciferase expression from both the DUX4 N3 motif and the murine DUX-type palindromic TGAT—ATCA P3, as well as from the palindromic TAAT—ATTA P3 motif, suggesting a broader DNA-binding spectrum for the ancestral protein compared to individual DUXC representatives from human and mouse (Figure 1H). Half-motif constructs (TAAT or TGAT alone) showed no activity, suggesting that sDUX binds cooperatively as a dimer to motifs with two core HD recognition sites. Furthermore, transactivation was detectable only at extremely low levels when motifs were present in a single copy, indicating

cooperativity of transactivation when multiple binding sites regulate a given promoter. In view of the sequence similarity between DUX and PAX HDs, a competitive interaction that has been described between DUX4 and PAX7,[8] and recent observations of a PAX7 profile that has been detected in FSHD muscle biopsy RNA-seq,[25,26] we also tested the PAX7 motif, which has TAAT cores but spaced by 2 nt, as well as variants in which one or both cores were TGAT. sDUX, like DUX4, had no activity on HD core motifs spaced by 2 nt.

As the activation domain of DUX4 is C-terminal, we tested the activity of an sDUX mutant lacking the C-terminal 74 amino acids. sDUXΔC was both non-toxic (Figure 1I) and unable to induce target genes (Figure 1J) indicating that its activation domain is localized within its C terminus and is necessary for cytotoxicity, like DUX4.[8,11] The reduction in activity was not due to reduced expression as the protein lacking the C terminus was actually expressed at slightly higher levels (Figure S1A). Because the C termini of DUX4 and sDUX do not show obvious sequence conservation, we tested their mechanistic similarity. One of the most unusual features of the DUX4 C terminus is that its expression leads to a global increase in nuclear H3K18 and H3K27 acetylation.[13,27] We found that cells expressing sDUX likewise displayed rapid and massive increases in total H3K18Ac and H3K27Ac (Figure 1K). The DUX4 activation domain is exquisitely dependent on the HAT activity of p300 and CBP.[27,28] We found that H3 acetylation driven by sDUX was reversed by treatment with iP300w (Figure 1K), a specific inhibitor of the HAT activity of p300 and CBP, as was the case for DUX4.[27] Likewise, transcriptional activation by sDUX was also suppressed by iP300w (Figure 1L), indicating that the activation domain of sDUX requires a p300/CBP cofactor, like that of DUX4.

Structural basis of sDUX DNA binding

To understand how sDUX could bind DUX4 targets when it has only a single HD, while DUX4 has two HDs of different core specificity, we tested the ability of bacterially produced sDUX protein to bind to double-stranded DNA bearing predicted recognition motifs using the electrophoretic mobility shift assay (EMSA). sDUX generated a pattern of band-shifts similar to that of DUX4 on both non-palindromic (TAAT—ATCA) and palindromic (TGAT—ATCA or TAAT—ATTA) motifs (Figure 2A). Although a weak band corresponding to sDUX monomer bound to DNA was observed at lower protein concentrations, sDUX bound to these DNA motifs primarily as a homodimer, suggesting high cooperativity. In contrast to the luciferase transcriptional assay, sDUX was also able to bind as a monomer to DNA substrates bearing either TAAT or TGAT half-motif, for which DUX4 shows no binding (Figure 2B). Similarly, sDUX bound as a monomer to the substrate with 2 nt separating TGAT and ATCA, incorrect spacing for DUX4 (Figures 2B and 2C). These results corroborate the results of the luciferase reporter assay that sDUX has a broader target DNA sequence selectivity, although they suggest that not all sites bound by sDUX *in vitro* (e.g., monomer sites) are transcriptionally active.

We then determined the crystal structure of the sDUX HD in complex with the non-palindromic DNA substrate that had previously been co-crystallized with the DUX4 double HD (Table S1).[24] As expected from the biochemical observations discussed earlier, sDUX binds to this target sequence as a head-to-head homodimer (Figure 2D). Except for the interdomain linker and the extended α-helix 3 of HD1, which are unique features for DUX4, the sDUX-DNA and DUX4-DNA complexes show overall very similar structures with a root-mean-square deviation (RMSD) of 0.75 Å for the protein backbone and all DNA atoms (Figure 2D). The two sDUX HDs interacting with the TAAT and TGAT half-sites also show high structural similarity, although they differ in the conformation of Arg75 from a characteristic basic patch near the C terminus of α-helix 3 (^{72}RRAR^{75}; Figure 1F). The side chain of Arg75 forms bidentate hydrogen bonds with the guanine base of 5′-TGAT-3′ in the major groove, while it shows alternative positioning in interacting with the 5′-TAAT-3′ motif (Figure 2E). This is reminiscent of the differential positioning of the corresponding Arg residues of DUX4 (Arg73 in HD1 and Arg148 in HD2) in the DUX4-DNA complex, which we previously showed is caused by a difference in key upstream residues (Glu70 in HD1 vs. Arg145 in HD2).[24]

Collectively, these data demonstrate that sDUX shows remarkable similarities to DUX4, including its primary architecture, mode of DNA binding, toxicity, DUX4 target gene expression, and p300 dependence, suggesting that the DUXC clade of the DUX family has retained the primary molecular properties of the ancestral gene at the root of the family.

DUXA and DUXB lack significant transcriptional activation potential

To understand the relationship of the A and B branches vis-à-vis C of the DUX family to sDUX, we next expressed the human DUXA and B proteins in human myoblasts, in their native form, and because their transactivation potential was uncertain due to the lack of C-terminal sequence conservation with the DUX4 transcriptional activation domain, we also fused them to a C-terminal VP64 activation domain;[29] we compared them to human DUXC (i.e., DUX4) and to sDUX (Figures S1B and S1C). Neither DUXA nor DUXB displayed any toxicity. Interestingly, however, the DUXA-VP64 fusion was toxic to human myoblasts. DUXB-VP64 was not (Figure 3A). We then evaluated the ability of these constructs to activate expression using luciferase reporters bearing two copies of the 3 flavors of DUX motif, as well as the PAX7 (P2 bearing 2 nt spacing) motif (Figures 3B and S2). DUXA and DUXB were both transcriptionally inactive in this assay, although the fusion to VP64 converted DUXA into an activator and revealed that DUXA recognizes both the P3 TGAT—ATCA murine DUX motif and the N3 TAAT—ATCA DUX4 motif equally well, and also, but more weakly, the P3 ATTA—ATTA motif, behaving very like sDUX in this assay. To evaluate the ability to induce DUX4 target genes, we performed RNA-seq on DUXA, B, VP64 derivatives and sDUX cells exposed to dox for 6 h, and unmodified cells, and compared to previously published data for DUX4 in the same system.[13] DUXA, DUXB, and DUXB-VP64 showed no induction of DUX4 target genes, whereas DUXA-VP64 and sDUX both showed a pattern of upregulation of these genes (Figures 3C and S3). These data strongly suggested that sDUX and DUXA may bind to many DUX4 target sites. DUXA apparently lacks a transcriptional activation domain of its own but acquires transactivation potential if provided with a heterologous activation domain at its C terminus.

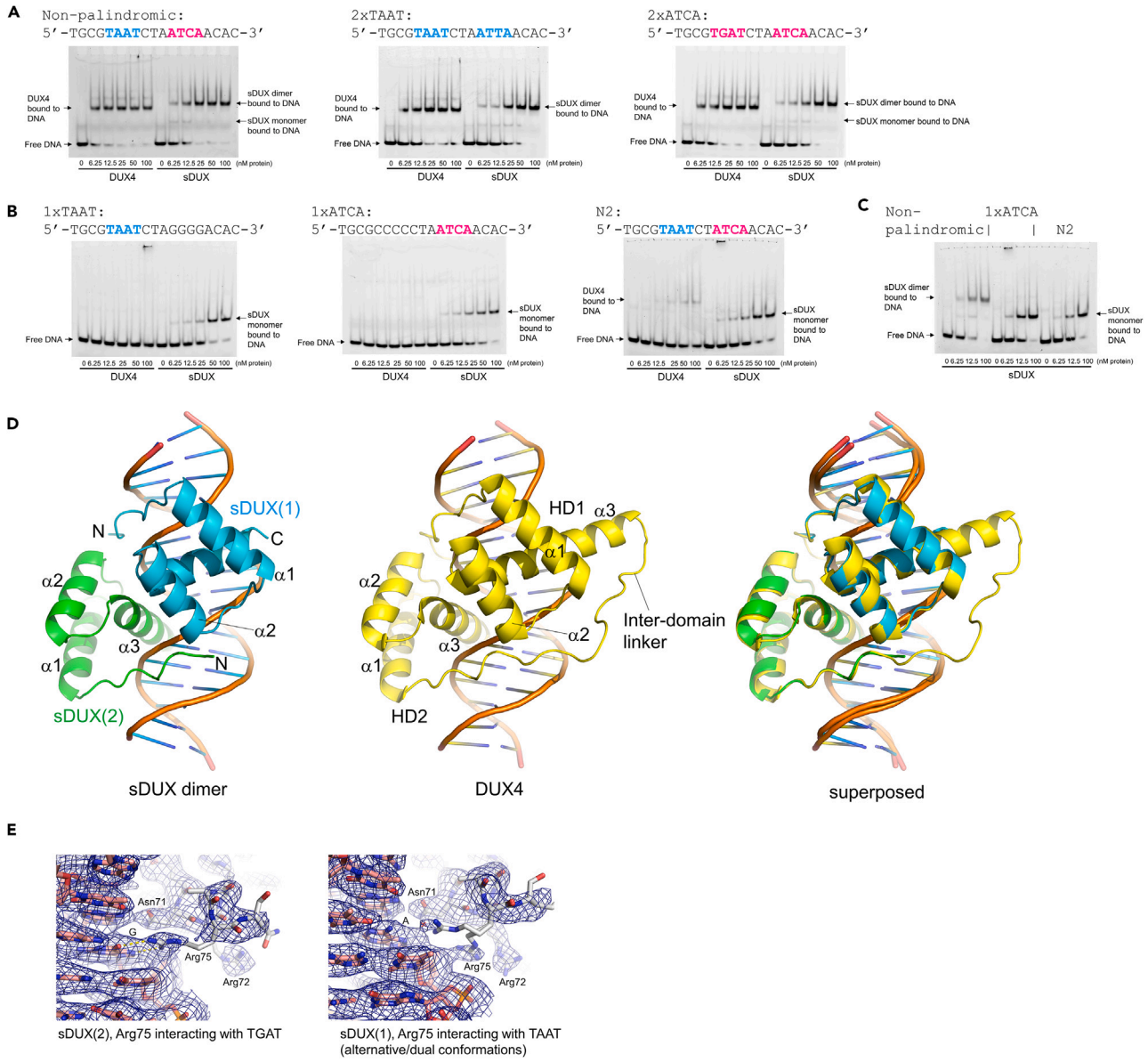

Figure 2. Structural basis of sDUX interaction with DNA

(A) Binding of DUX4 HD1-HD2 and sDUX HD to the non-palindromic (TAAT—ATCA) and palindromic (TGAT—ATCA or TAAT—ATTA) motifs tested in EMSA. All DNA substrates were double-stranded DNA. Sequence of the fluorescently labeled strand is shown above each gel. Gels are representative of duplicates.

(B) Binding of DUX4 HD1-HD2 and sDUX HD to the TAAT and TGAT half-motifs or a non-palindromic motif with 2 nt spacing (N2) tested in EMSA. Gels are representative of duplicates.

(C) Binding of sDUX HD to the three different types of DNA substrates, highlighting distinct mobilities of dimeric vs. monomeric complex in EMSA.

(D) Crystal structure of sDUX homodimer bound to the non-palindromic target motif with 3 nt spacing, the structure of DUX4 double homeodomain with the same DNA substrate as reported previously,[24] and their superposition.

(E) Differential interaction of sDUX Arg75 with the TAAT and TGAT motifs in the crystal structure. 2Fo-Fc electron density for the structure with Br-dU-containing DNA is shown as blue mesh, contoured at 0.9 σ.

DUXA-VP64 interferes with myogenesis

One of the hallmark activities of DUX4 is inhibition of myogenesis,[8] and this is associated with its ability to perturb (primarily by downregulation) myogenic gene expression.[9] We therefore evaluated the set of myogenic genes perturbed by DUX4[9] within the profiles of each DUX family member (Figure 3D). While native DUXA and DUXB had virtually no effect on these genes, sDUX and DUXA-VP64 showed DUX4-like perturbations of many of these genes, including the key master regulator, *MYOD1*, which was strongly downregulated by both factors. This again indicates the similarity of sDUX to DUX4 and further suggests that DUXA may have a biologically meaningful degree of overlap in DNA

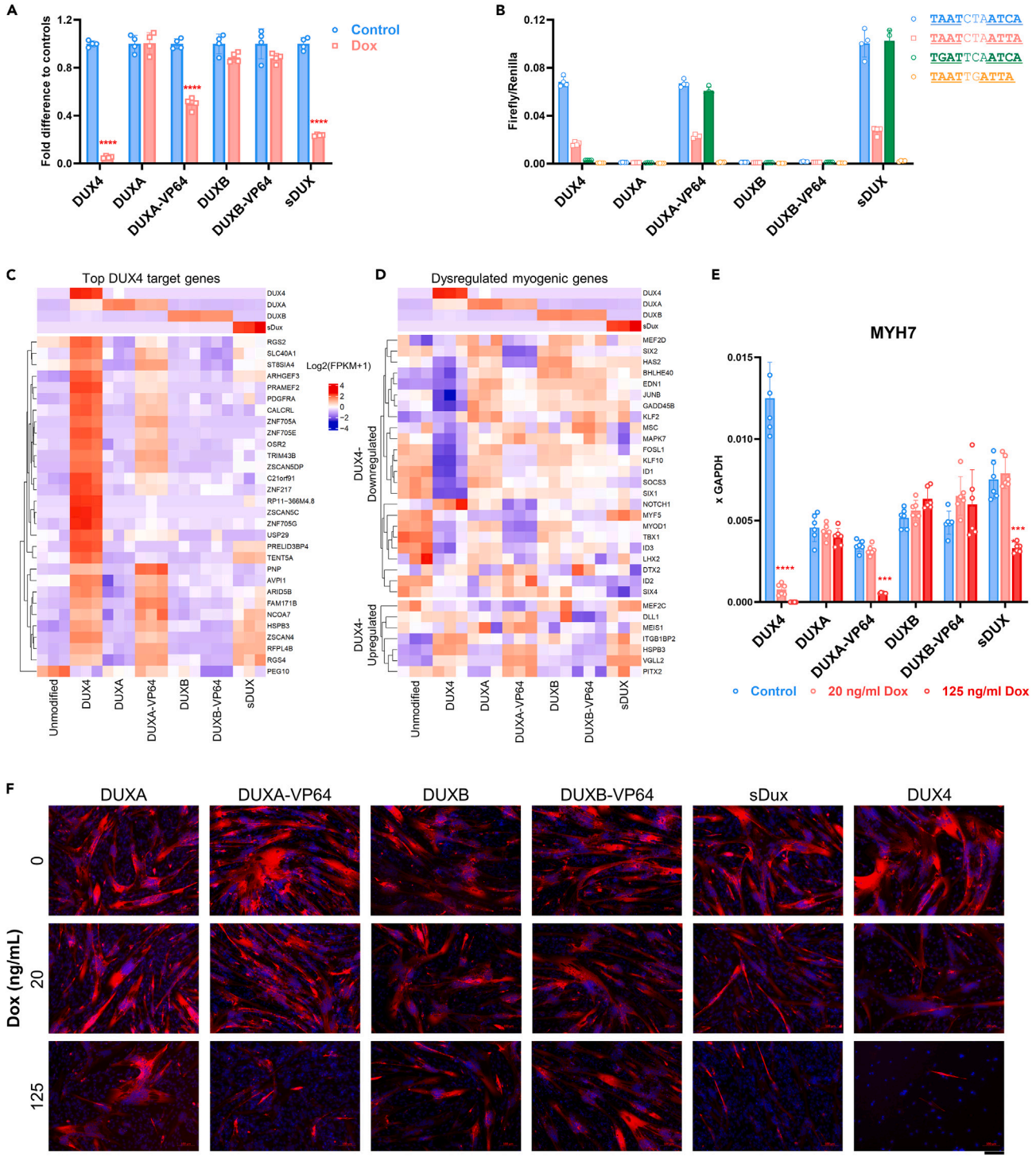

Figure 3. Toxicity and myogenic differentiation effects of DUX family members and VP64-fusions

(A) Viability (ATP) assay in LHCN-M2 human myoblasts after 96 h of expression of different DUX family proteins induced with 200 ng/mL doxycycline. Data are presented as fold difference to the control (uninduced cells); n = 4.

(B) Luciferase assays in 293T cells induced with 1 μg/mL dox for 24 h to express various DUX family proteins and VP64 derivatives on the 3 versions of DUX motif (N3 and P3) as well as a motif with spacing of 2 nt (P2-type). Data are presented as mean ± SEM; n = 4.

(C) Heatmap of the top DUX4 target genes showing expression in cells expressing various DUX family members and VP64 derivatives after 12 h of induction (200 ng/mL dox) in LHCN-M2 human myoblasts.

Figure 3. *Continued*

(D) Heatmap of the top myogenic genes affected by DUX4, and the effect of other DUX family members, and DUXA- and DUXB-VP64 activation domain fusions on this set. Genes downregulated by DUX4 shown above; genes upregulated by DUX4 shown below. LHCN-M2 human myoblasts carrying inducible gene of interest were induced by 200 ng/mL dox for 12 h.

(E) Real time RTqPCR for MYH7, a marker of differentiation, after differentiation with 72 h of expression of different DUX family proteins at 20 or 125 ng/mL dox. Data are presented as mean ± SEM; ***p < 0.01**, ****p < 0.0001 by one-way ANOVA, n = 6.

(F) Representative immunostaining for sarcomeric myosin heavy chain on the same cells shown in panel e. Nuclei are counterstained with DAPI. Scale bar is 100 nm.

binding with DUX4, revealed here by converting it into an activator by fusion to VP64, whereas DUXB does not. To test the phenotypic effect of these myogenic changes, we subjected the cell lines to differentiation in the presence of dox. DUXA-VP64 and sDUX both showed suppression of *MYH7*, a differentiation marker, as well as of morphological differentiation to multinucleated pan-myosin heavy chain+ myotubes, similar to DUX4 (Figures 3E and 3F).

Transcription and chromatin profiling reveals relationships among DUX family proteins

In order to definitively evaluate the regulatory potential of DUX family members, we performed RNA-seq in both the presence and absence of a 12-h pulse of dox on DUX4, DUXA, DUXB, DUXA-VP64, and sDUX. Principal-component analysis showed transcriptional profiles of all cell lines in the absence of dox to be clustered, with the exception of DUX4, which showed a leftward shift on PC1, the axis that contains 62% of variance among all conditions (Figure 4A). Dox induction led to a much greater left shift for DUX4, indicating that the leftward shift of the control reflects very low background expression of DUX4 targets in the absence of dox. In the presence of dox, both DUXA and DUXB remained close to the cluster containing the negative controls, supporting the notion that they are transcriptionally inactive. Both sDUX and DUXA-VP64 showed a degree of similarity to DUX4 in the form of a slight leftward shift on PC1 (where most variance is contained), but also an upward shift on PC2 (which contains only 8% of the variance). This indicates that there are unique aspects of the sDUX profile that DUXA-VP64 participates in but DUX4 does not. The relationships between the expression profiles of sDUX, DUX4, and DUXA-VP64 are striking (Figure 4B; Table S2) with significant overlapping gene sets (Figure 4C). A large fraction of the genes induced by each factor in human myoblasts comprises genes expressed up to and during the human 8-cell stage,[30] here referred to as ZGA genes (sDUX, 119 of 671, 18%; DUXA-VP64, 101 of 629, 16%; DUX4 436 of 2,523, 17%). Within the ZGA gene set, there is slightly larger overlap; for example, 74% of the sDUX ZGA targets are co-regulated by DUX4 (vs. 64% of all targets) as are 70% of the DUXA-VP64 ZGA targets (vs. 45% of all targets). Repetitive elements, especially LTR-like repeats, are prominently and specifically expressed in early cleavage stages[31] and represent a significant set of ZGA-related targets of DUX4 and mouse DUX. We found that both sDUX and DUXA-VP64 induced transcription of repetitive elements, with LTR-type elements being most abundant among these, and sDUX sharing with DUX4 the ability to induce LINE elements (Figure 4D). Strong correlations were seen among the transcriptional profiles of sDUX, DUX4, and DUXA-VP64 in both conventional genes (Figure 4E, upper left) and repetitive elements (Figure 4E, lower right); with the greatest correlations being between sDUX and DUX4 (Figures 4F and 4G).

We next investigated global chromatin changes with assay for transposase-accessible chromatin with sequencing (ATAC-seq) on the same set of cells after 12 h of dox exposure to induce expression of DUX proteins. ATAC-seq peak profiles for the control untreated cells clustered together, and again, major differences after dox induction were observed only with DUX4, sDUX, and DUXA-VP64, while DUXA and DUXB continued to cluster with the controls, although DUXA showed a greater change in response to dox than DUXB (Figure 5A; Table S3). Numerous co-localized dox-induced peaks near ZGA genes were found, for example *ZSCAN4* and *PRAMEF12*, in which DUX4, sDUX, DUXA-VP64, as well as DUXA peaks overlapped (Figures 5B and 5C). Interestingly, the *DUXA* gene itself showed a remarkable increase in chromatin accessibility induced by DUX4, vis-à-vis the other factors (Figure S4).

Interrogating peaks for the presence of overrepresented sequence motifs revealed variants of the 11 bp motifs previously associated with DUX4[10] and mouse DUX[32] (Figure 5D). Notably, DUX4 motifs preferred A in position 2, while DUXA-VP64 and sDUX preferred A or G equally in position 2 (Figure 5D), in clear agreement with their respective luciferase reporter assays (Figure 3B). Evaluating the simple pattern of two 4 nt cores of either TAAT or TGAT separated by any 3 nucleotides within peak sets revealed a clear preference for P3 TGAT by sDUX and DUXA-VP64, while P3 TAAT and N3 patterns were more frequent in DUX4 peaks, with the majority of DUX4 peaks bearing the N3 pattern (Figure 5E). Enumerating the preferred motifs for each factor within their peak set revealed that the majority of dox-induced ATAC-seq peaks had at least one motif, with close to 50% having 2 or more (Figure 5F).

Combining the RNA-seq with ATAC-seq to identify ATAC-seq peaks near genes upregulated by each factor, we evaluated the state of chromatin over each peak before and after dox treatment. Peaks that were induced only by DUX4 and not by sDUX or DUXA-VP64 tended to be completely closed prior to dox induction (Figure 5G, second row). The same was not true for sDUX- or DUXA-VP64-specific peaks (Figure 5G, first and third rows), or for shared peaks, which tended to be open prior to factor expression. This suggests that these factors are less able to bind regions of closed chromatin, while DUX4 has a potent pioneering activity. Interestingly, DUX4-specific peaks tended to have a weak signal for sDUX binding, suggesting that sDUX may also have a modicum of pioneer activity.

DUXA inhibits DUX4 activity

Because *DUXA* is strongly induced by DUX4, because DUXA-VP64 acts on many of the same genes as DUX4, and because in its native form, DUXA lacks transcriptional activation potential, it seemed possible that DUXA might participate in negative feedback regulation of DUX4 activity by competing with DUX4 for binding sites that regulate key target genes. To directly investigate sites of DNA binding of DUXA and DUX4, we

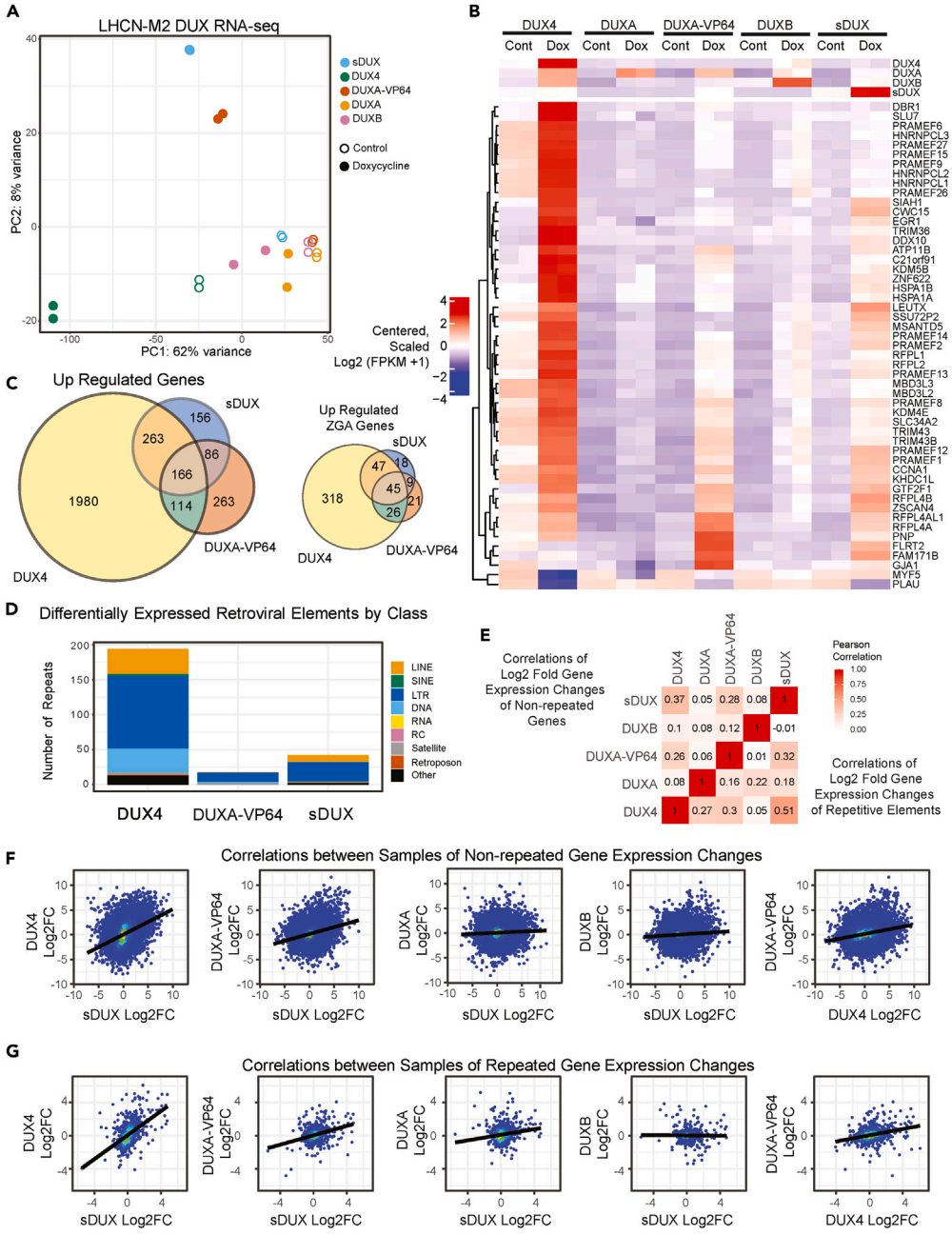

Figure 4. Transcriptional profiles of DUX family members

(A) Principal-component analysis of gene expression profiles in the absence (open circles) and presence (closed circles) of 200 ng/mL dox for 12 h. DUX4 expressing cells are strongly shifted along PC1 which accounts for 62% of the variance while DUXA-VP64 and sDUX-expressing cells are more prominently shifted along PC2 which contains 8% of the variance.

(B) Heatmap representation of log2 transformed FPKM values for the top 50 differentially expressed genes among all factors. Expression of *DUX4*, *DUXA*, *DUXB*, and *sDUX* is shown in the upper panel.

(C) Venn diagrams showing overlap in upregulated gene sets among total genes (left) and ZGA genes (right). Upregulated genes for each set were defined as having a greater than 2-fold change, and Benjamini-Hochberg adjusted p value less than 0.05 and a mean FPKM value >2.5 in the dox-induced sample.

(D) Distribution of repeat classification among the differentially expressed retroviral elements for DUX4, DUXA-VP64 and sDUX. Differentially expressed elements were defined as being upregulated or downregulated greater than 2-fold and having a Benjamini-Hochberg adjusted p value less the 0.05.

(E) Pearson correlations of log2 fold changes in expression upon induction with dox between each of the DUX factor. The upper left half of the matrix corresponds to conventional genes whereas the lower right half of the matrix corresponds to log2 fold changes for repetitive elements.

Figure 4. *Continued*

(F) Scatterplots of the log2 fold changes in conventional expression between DUX factors. Points representing individual genes are colored according to density to show the higher density of points near the center. A linear fit of each correlation is shown as a black line.

(G) Scatterplots similar to panel (F) for repetitive elements.

performed chromatin immunoprecipitation sequencing (ChIP-seq) with epitope-tagged versions of DUXA and DUX4 in 293T cells and evaluated peaks for overlap (Figure 6A). As the ATAC-seq data and motif analysis suggested, there was substantial overlap in DNA binding among these two factors (Figures 6B and 6C). Approximately 70% of 1,989 genes with a nearby DUX4 peak also showed a nearby DUXA peak (Figure 6C).

We then tested whether DUXA could inhibit the activity of DUX4 by overexpressing DUXA constitutively in dox-inducible DUX4 expressing human myoblasts. Cells overexpressing DUXA showed a diminished ability of DUX4 to induce all of the targets we tested, compared to controls (Figure 6D). As a further test of specificity, we knocked down DUXA in the constitutively expressing cell lines and observed the reversal of the DUXA effect. The activity of DUXA in suppressing DUX4 activity was independently replicated in another wild-type (WT) immortalized human myoblast cell line and in the context of pulsed DUX4 expression as opposed to continual expression (Figure S5).

DUXA activity in FSHD patient-derived myoblasts

To evaluate the potential relevance of this effect in FSHD, we performed a similar experiment on an immortalized myoblast line from an FSHD-affected patient. In this case, the source of DUX4 is the endogenous DUX4 locus, and we delivered DUXA on a dox-inducible lentivirus. Because DUX4 target gene expression is strongly associated with differentiation, we differentiated these cells in the presence of dox added and compared DUX4 target gene expression levels to those of cells differentiating under normal conditions (Figure 6E). DUXA did not cause any significant morphological aberration in WT or FSHD cells. These data reveal that also in FSHD cells, where DUX4 is expressed in a disease-relevant way, DUXA can inhibit the expression of DUX4 target genes.

DISCUSSION

Because of the genetic divergence between the 3 clades of the DUX gene family, and the fact that the DUXC clade has acquired a tandem duplication amplification which has been retained (i.e., selected for) in all DUX family-bearing eutherian mammalian genomes evaluated,[2] it seemed most probable that the double HD proteins of the DUXC clade represent a neomorphic activity—a functional innovation over their ancestral single HD progenitor. It was thus highly surprising that sDUX behaves like DUX4 in its cellular phenotypes of cytotoxicity and inhibition of myogenic differentiation and that, despite lacking C-terminal sequence conservation, sDUX has a C-terminal p300/CBP-dependent activation domain and indeed has significantly overlapping downstream targets with DUX4, including a large number of ZGA-specific target genes. Rather than acquiring a neomorphic mutation, the DUXC clade seems to have retained the original function of sDUX, while the A and B clades represent loss of function or indeed antimorphic innovations.

The similarity in cytological phenotypes between sDUX and DUX4 is due in part to the similarity in the way these proteins bind DNA. Although sDUX has a single HD, we find here that it binds DNA as a head-to-head dimer, in a nearly identical fashion to the head-to-head conformation of the tandem DUX4 HDs.[24] This is in spite of a key difference, the lack of the interdomain linker of DUX4, which makes contacts with the DNA minor groove in the gap between the two core 4 nt sequences as well as at additional sites along the 11 nt motif (TAATCTAATCA), and which constrains the freedom of movement of the two HDs. Like DUX4, sDUX had no activity on HD core motifs spaced by 2 nt, suggesting that cooperative binding requires the 3 nt spacing. In this regard, it would be interesting to test whether DUX4 HD2 in isolation exhibits relaxed sequence selectivity as sDUX and, conversely, whether sDUX placed in a tandem HD context would show higher selectivity than the non-covalent sDUX homodimer in DNA binding. Of note, mutants of DUX4 lacking the first HD[33] and a naturally occurring splice variant that disrupts HD1 in canines, DUXC-alt,[34] are inactive, demonstrating that DUXC HDs have most likely lost the ability to homodimerize.

Regarding the specific sequence preferences of DUX proteins, it was previously demonstrated that although human and mouse DUXC proteins (DUX4 and DUX, respectively) recognize very similar 11 nt motifs, human DUX4 prefers the N3 (non-palindromic) TAAT—ATCA pattern against murine DUX, which prefers a P3 TGAT—ATCA pattern. The orientation of Glu70 in helix 3 of DUX4 HD1 specifies TAAT preference, and this orientation was variable in sDUX allowing it to bind TAAT and TGAT equally well. We infer that the relaxed sequence preference is an intrinsic feature of DUX proteins, likely derived from the ancestral HD, and that human and mouse DUXC specificity for the non-palindromic vs. palindromic subsets is a derived feature. It will therefore be important to evaluate DUXC proteins from other species to determine whether evolved selectivity of motif recognition is an intrinsic feature of the DUXC clade, or whether human and mouse DUXC represent exceptions to the general pattern exemplified by sDUX. Irrespective of their idiosyncrasies, it is important to point out that both DUX4 and mouse DUX have the same basic cytotoxic phenotypes[32,35] and effects on differentiation,[35] as indeed do sDUX and DUXA-VP64, whose sequence preferences encompass both those of DUX4 and DUX; thus, the key function of these proteins is probably retained in their shared downstream targets, of which there are many,[14] rather than those targets that are differentially regulated due to their evolved specificity.

If the DUXC clade retains the key properties of sDUX, what is the role of the DUXA and DUXB genes? Both DUXA and DUXB are transcriptionally inactive; however, adding the VP64 activation domain revealed that DUXA acquired the DUX4 properties of cytotoxicity and inhibition of myogenic differentiation and that it could regulate many DUX4 target genes, an interpretation strongly supported by the large overlap of DUXA and DUX4 ChIP-seq sites near DUX4-regulated genes. DUXB on the other hand was either unable to bind DNA in the context of our studies or not converted into an activator by fusion to VP64, as it showed extremely limited activity in these assays. Thus, despite DUX4, sDUX, and DUXA-VP64 each having many unique targets, they all 3 share a large set of common targets, suggesting that the common phenotype of

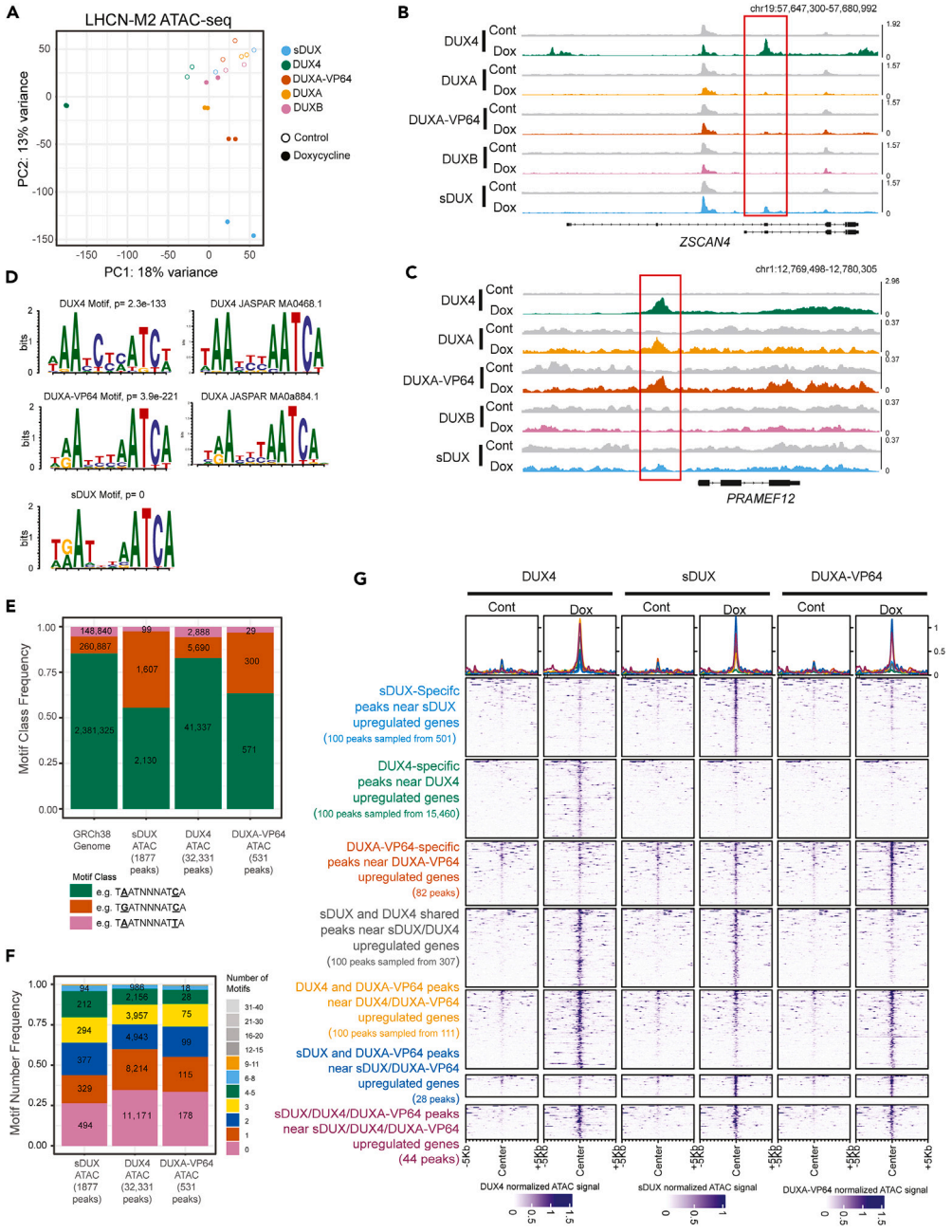

Figure 5. Chromatin changes induced by DUX family members

(A) Principal-component analysis of ATAC-seq data in the absence (open circles) and presence (closed circles) of 200 ng/mL dox for 12 h. Called peaks from each factor were combined into a composite set of genomic locations that had changes in DNA accessibility in one or more samples. A matrix of the number of reads within each region across all the samples was used to calculate the principal components.

(B) ATAC-seq coverage tracks for each DUX factor at the *ZSCAN4* locus in the absence (gray) or presence (colored according to panel a) of dox. Each track shown is a combination of two biological replicates normalized to the total number of reads per million. The scale for each pair of tracks is shown at the right, and the gene structure is shown below. The red box corresponds to peaks that appear for some DUX factors upon the addition of dox.

(C) ATAC-seq coverage similar to panel B for the *PRAMEF12* locus.

(D) The DNA sequences from the top 500 peaks were used to define *de novo* motifs for DUX4, DUXA-VP64, and sDUX. The top motif and its p value are shown. The DUX4 and DUXA-VP64 motifs are similar to the previously defined motifs for DUX4 and DUXA repectively (https://jaspar.genereg.net/).

(E) The *de novo* motifs identified from the top 500 DUX4, DUXA-VP64, and sDUX peaks were identified across each dataset using a 95% scoring threshold. Classification of each sequence is based on the nucleotide at the 2nd and 10th position.

Figure 5. *Continued*

(F) The number of sequence motifs identified in panel e per ATAC-seq peak was counted to show that peaks frequently contain multiple copies of the DUX motif in all three datasets.

(G) Heatmaps of ATAC-seq coverage for peaks within 10 kb of an upregulated gene. Peaks were classified into one of seven groups depending on whether they were unique to a particular dataset or shared between two or more datasets. Groups that contained more than 100 peaks were randomly subsampled to 100 peaks. Coverage was normalized to total counts per million reads of each dataset and then plotted on the scale defined by the dox-induced dataset shown below the heatmaps.

cell death and inhibition of myogenic differentiation resides in this set of common transcriptional targets. DUXA in its native form of course fails to induce these targets. By binding a set of sites associated both with ZGA and with phenotypic cytotoxicity, but failing to induce them, DUXA inhibits the activity of DUX4. Importantly, DUXA is one of the most potently and rapidly upregulated targets of DUX4, suggesting a feedback-inhibitory mechanism. Such feedback inhibition would serve to limit the temporal effect of a burst of DUX4 expression, explaining why the burst of DUX4 target genes in ZGA is so brief. We note that such a negative feedback role is also demonstrated for mouse DUXBL against mouse DUX in a companion study.[36] This feedback inhibition model stands in stark contrast to the previously suggested idea that DUXA serves to amplify or maintain the DUX4 signal after a burst of DUX4.[23] Although a positive feedback role for DUXA was attractive in explaining persistent effects of DUX4 long after a burst of expression, it would be incompatible with early embryogenesis and it is inconsistent with the data shown in the current study.

Inhibition of DUX4 by DUXA has implications for disease states involving DUX4. In FSHD, where DUX4 is potentially driving cytotoxicity or impairing myogenic regeneration, DUXA levels would serve as a rheostat on DUX4 activity and therefore limit the phenotype. Variation in DUXA levels among individuals, as well as among tissues, is thus of relevance in this disease of extremely variable penetrance and expressivity. Interestingly, a frameshifted version of DUX4 referred to as DUX4C which alters the C terminus has also been shown to antagonize the ability of DUX4 to induce expression of its target genes when overexpressed;[37] thus, variations in DUX4C expression levels could theoretically contribute to such a rheostat. Likewise, in cancers that show evidence of DUX4 expression,[20] DUXA will serve to limit DUX4 activity on certain targets. The antagonistic relationship between DUXC and DUXA/DUXBL means that the mechanisms operating downstream of DUX4 in cancers in which DUX4 expression has been detected are not the same as the mechanisms that allow DUXBL to promote rhabdomyosarcoma.[21]

These studies thus demonstrate that far from being a set of genes of similar activity, the DUX family of genes encode proteins of opposing function, namely the DUXC clade with potent p300/CBP-dependent transcriptional activity, the DUXA and B clades, which lack transcriptional activation potential, and DUXA, which serves to competitively constrain in a feedback-inhibitory manner, the activity of DUXC proteins like DUX4. This understanding serves to explain the extreme temporal limitation of activity of DUX4 and mouse DUX at ZGA and informs the interpretation of DUX4 and DUXA expression in cancer and FSHD.

Limitations of the study

This study investigates the activity of the human DUX proteins in cell lines cultured *in vitro*. As such, speculations about the function of these proteins *in vivo* are extrapolations. Formal proof of activity in humans would require *in vivo* experiments, ethically not feasible, although we do show that DUXA inhibits DUX4 in myoblasts from an FSHD patient (Figure 6E). *In vivo* activity studies in another eutherian animal model such as mouse would provide valuable information, although outside the scope of the current study, which focuses on the human genes.

STAR★METHODS

Detailed methods are provided in the online version of this paper and include the following:

- KEY RESOURCES TABLE
- RESOURCE AVAILABILITY
  - Lead contact
  - Materials availability
  - Data and code availability
- EXPERIMENTAL MODEL AND STUDY PARTICIPANT DETAILS
- METHOD DETAILS
  - Synthesis of expression constructs
  - Cell culture
  - RNA interference
  - EdU incorporation
  - Annexin V/7-AAD staining
  - Transduction
  - Cell viability (ATP) assay
  - Dual Glo luciferase assay
  - mRNA generation and transfection
  - Western blots
  - RNA isolation, quantitative real time RT-PCR (RTqPCR) and RNAseq

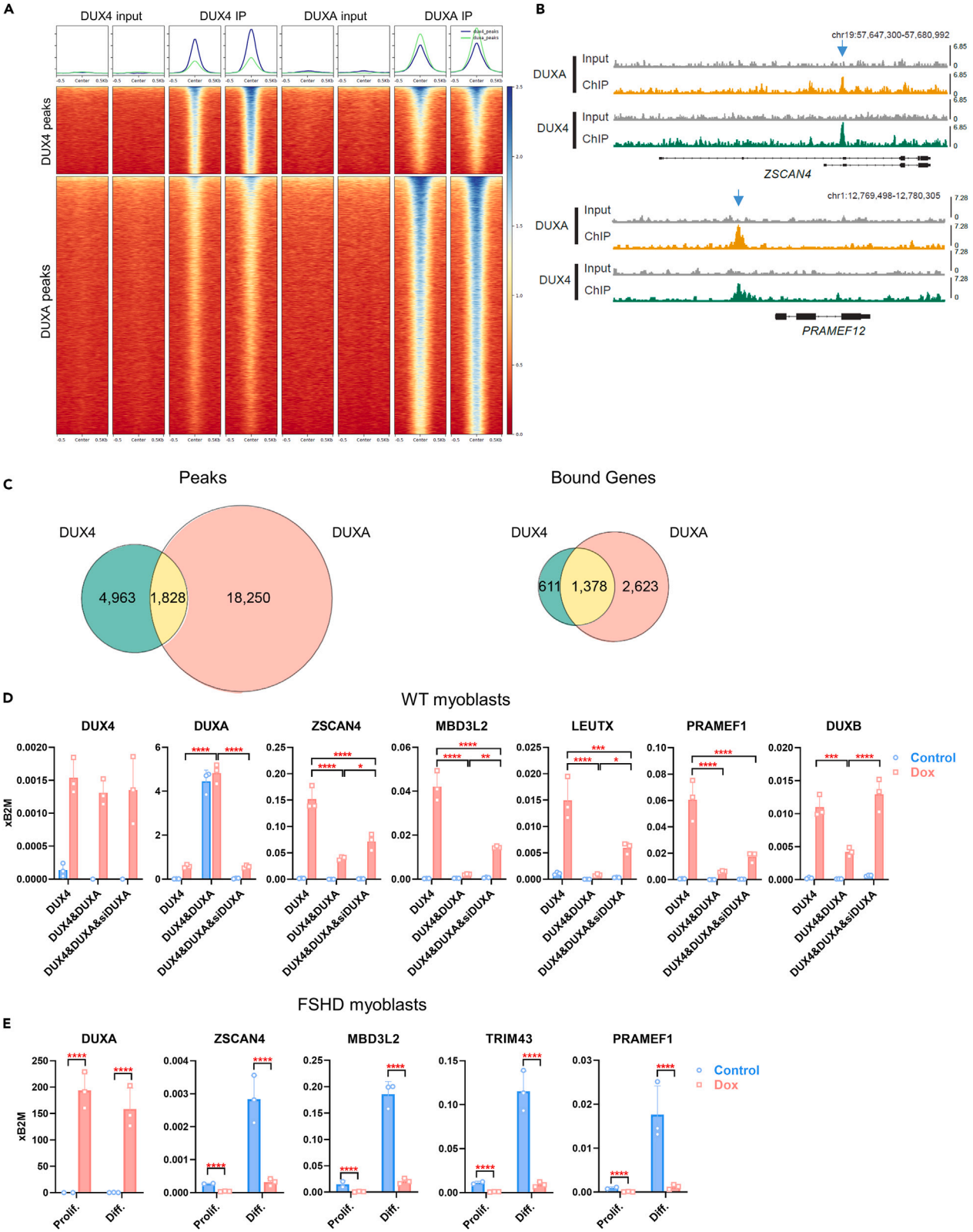
A
DUX4 input
DUX4 IP
DUXA input
DUXA IP
DUX4 peaks
DUXA peaks
B
chr19:57,647,300-57,680,992
DUXA
Input
ChIP
DUX4
ZSCAN4
chr1:12,769,498-12,780,305
PRAMEF12
C
Peaks
DUX4
DUXA
4,963
1,828
18,250
Bound Genes
611
1,378
2,623
D
WT myoblasts
DUX4
DUXA
ZSCAN4
MBD3L2
LEUTX
PRAMEF1
DUXB
xB2M
Control
Dox
DUX4
DUX4&DUXA
DUX4&DUXA&siDUXA
E
FSHD myoblasts
DUXA
ZSCAN4
MBD3L2
TRIM43
PRAMEF1
xB2M
Control
Dox
Prolif.
Diff.

Figure 6. DUXA binds many DUX4 targets and inhibits DUX4 transcriptional activity

(A) Tornado plots aligning on peak centers for called DUX4 peaks (upper panel) and DUXA peaks (lower panel) for both input and IP samples for both experiments. Overlap of DUX4 and DUXA peaks (peak calling: FDR $\leq$ 0.1, minimum treatment reads $\geq$ 1, enrichment $\geq$ 1, log10 (q value) $\leq$ −0.5; not overlapping blacklisted regions like satellite repeats or misassemblies (ENCODE).

(B) ChIP-seq coverage tracks for DUXA and DUX4 surrounding the *ZSCAN4* (upper) and *PRAMEF12* (lower) genes. Input tracks are shown in gray and IP tracks are colored uniquely. Each track shown is a combination of two normalized biological replicates. The scale for each track is shown at the right and the gene structure is shown below. Arrows indicate shared peaks.

(C) Venn diagrams showing overlap in peaks (left) and in bound genes (right). Promoter = gene TSS + upstream 5000 nt + downstream 5000 nt; overlap of $\geq$1 nt.

(D) Real time RTqPCR for DUX4 target genes in LHCN-M2iDUX4 immortalized human WT myoblasts co-expressing either DUXAiresEGFP or EGFP control, and cells in which overexpressed DUXA was knocked down by siRNA or control non targeted siRNA. Cells were induced with 200 ng/mL doxycycline for 8 h. Data are presented as mean ± SEM; ***p < 0.001, ****p < 0.0001 by two-way ANOVA, n = 3.

(E) Real time RTqPCR for DUX4 target genes in immortalized human FSHD myoblasts engineered for dox-inducible for DUXA (M008-iDUXA). Cells were induced with 200 ng/mL doxycycline for 48 h in proliferation conditions (Prolif.). For differentiation (Diff.), cells were cultured in differentiation medium for 3 days. DUXA was induced (200 ng/mL dox) over the last 24 h of differentiation. Data are presented as mean ± SEM; ****p < 0.0001 by two-way ANOVA, n = 3.

SUPPLEMENTAL INFORMATION

Supplemental information can be found online at https://doi.org/10.1016/j.isci.2023.107823.

ACKNOWLEDGMENTS

We thank Jasmine Gulik, Ana Mitanoska, David Oyler, Natalie Xu, and MacKenzie Molina for the help with molecular analyses. We thank Cynthia Faraday for graphic art. This work was supported by grants from the National Institute of Arthritis and Musculoskeletal and Skin Diseases (R01 AR055685 to M.K., and R01 AR081228 to D.B.), the National Institute of General Medical Sciences (R35 GM118047 to H.A.), and the FSHD Society (2022-2212350103 to D.B.). X-ray diffraction data were collected at the Northeastern Collaborative Access Team beamlines, which are funded by the US National Institutes of Health (NIGMS P30 GM124165). The Pilatus 6M detector on 24-ID-C beamline is funded by an NIH-ORIP HEI grant (S10 RR029205). This research used resources of the Advanced Photon Source, a U.S. Department of Energy (DOE) Office of Science User Facility operated for the DOE Office of Science by Argonne National Laboratory under Contract No. DE-AC02-06CH11357. The monoclonal antibody against MHC was obtained from the Developmental Studies Hybridoma Bank, developed under the auspices of the NICHD and maintained by the University of Iowa.

AUTHOR CONTRIBUTIONS

Experimentation: DB, EAT, ETE, MDG, LY, FL, AM, KSS.

Writing: DB, MDG, JK, HA, MK.

DECLARATION OF INTERESTS

The authors declare no competing interests.

Received: February 6, 2023
Revised: July 7, 2023
Accepted: August 31, 2023
Published: September 2, 2023

REFERENCES

1. Clapp, J., Mitchell, L.M., Bolland, D.J., Fantes, J., Corcoran, A.E., Scotting, P.J., Armour, J.A.L., and Hewitt, J.E. (2007). Evolutionary conservation of a coding function for D4Z4, the tandem DNA repeat mutated in facioscapulohumeral muscular dystrophy. Am. J. Hum. Genet. *81*, 264–279.
2. Leidenroth, A., and Hewitt, J.E. (2010). A family history of DUX4: phylogenetic analysis of DUXA, B, C and Duxbl reveals the ancestral DUX gene. BMC Evol. Biol. *10*, 364–1471. https://doi.org/10.1186/1471-2148-10-364.
3. Gabriëls, J., Beckers, M.C., Ding, H., De Vriese, A., Plaisance, S., van der Maarel, S.M., Padberg, G.W., Frants, R.R., Hewitt, J.E., Collen, D., et al. (1999). Nucleotide sequence of the partially deleted D4Z4 locus in a patient with FSHD identifies a putative gene within each 3.3 kb element. Gene *236*, 25–32. https://doi.org/10.1016/s0378-1119(99)00267-x.
4. van Overveld, P.G.M., Lemmers, R.J.F.L., Sandkuijl, L.A., Enthoven, L., Winokur, S.T., Bakels, F., Padberg, G.W., van Ommen, G.J.B., Frants, R.R., et al. (2003). Hypomethylation of D4Z4 in 4q-linked and non-4q-linked facioscapulohumeral muscular dystrophy. Nat. Genet. *35*, 315–317.

5. Snider, L., Geng, L.N., Lemmers, R.J.L.F., Kyba, M., Ware, C.B., Nelson, A.M., Tawil, R., Filippova, G.N., van der Maarel, S.M., Tapscott, S.J., et al. (2010). Facioscapulohumeral dystrophy: incomplete suppression of a retrotransposed gene. PLoS Genet. *6*, e1001181. https://doi.org/10.1371/journal.pgen.1001181.
6. Wijmenga, C., Hewitt, J.E., Sandkuijl, L.A., Clark, L.N., Wright, T.J., Dauwerse, H.G., Gruter, A.M., Hofker, M.H., Moerer, P., Williamson, R., et al. (1992). Chromosome 4q DNA rearrangements associated with facioscapulohumeral muscular dystrophy. Nat. Genet. *2*, 26–30.
7. Kowaljow, V., Marcowycz, A., Ansseau, E., Conde, C.B., Sauvage, S., Mattéotti, C., Arias, C., Corona, E.D., Nuñez, N.G., Leo, O., et al. (2007). The DUX4 gene at the FSHD1A locus encodes a pro-apoptotic protein. Neuromuscul. Disord. *17*, 611–623.
8. Bosnakovski, D., Xu, Z., Gang, E.J., Galindo, C.L., Liu, M., Simsek, T., Garner, H.R., Agha-Mohammadi, S., Tassin, A., Coppée, F., et al. (2008). An isogenetic myoblast expression screen identifies DUX4-mediated FSHD-associated molecular pathologies. EMBO J. *27*, 2766–2779. https://doi.org/10.1038/emboj.2008.201.
9. Bosnakovski, D., Gearhart, M.D., Toso, E.A., Ener, E.T., Choi, S.H., and Kyba, M. (2018). Low level DUX4 expression disrupts myogenesis through deregulation of myogenic gene expression. Sci. Rep. *8*, 16957. https://doi.org/10.1038/s41598-018-35150-8.
10. Geng, L.N., Yao, Z., Snider, L., Fong, A.P., Cech, J.N., Young, J.M., van der Maarel, S.M., Ruzzo, W.L., Gentleman, R.C., Tawil, R., et al. (2012). DUX4 activates germline genes, retroelements, and immune mediators: implications for facioscapulohumeral dystrophy. Dev. Cell *22*, 38–51. https://doi.org/10.1016/j.devcel.2011.11.013.
11. Kawamura-Saito, M., Yamazaki, Y., Kaneko, K., Kawaguchi, N., Kanda, H., Mukai, H., Gotoh, T., Motoi, T., Fukayama, M., Aburatani, H., et al. (2006). Fusion between CIC and DUX4 up-regulates PEA3 family genes in Ewing-like sarcomas with t(4;19)(q35;q13) translocation. Hum. Mol. Genet. *15*, 2125–2137. https://doi.org/10.1093/hmg/ddl136.
12. Bosnakovski, D., Lamb, S., Simsek, T., Xu, Z., Belayew, A., Perlingeiro, R., and Kyba, M. (2008). DUX4c, an FSHD candidate gene, interferes with myogenic regulators and abolishes myoblast differentiation. Exp. Neurol. *214*, 87–96. https://doi.org/10.1016/j.expneurol.2008.07.022.
13. Choi, S.H., Gearhart, M.D., Cui, Z., Bosnakovski, D., Kim, M., Schennum, N., and Kyba, M. (2016). DUX4 recruits p300/CBP through its C-terminus and induces global H3K27 acetylation changes. Nucleic Acids Res. *44*, 5161–5173. https://doi.org/10.1093/nar/gkw141.
14. Hendrickson, P.G., Doráis, J.A., Grow, E.J., Whiddon, J.L., Lim, J.W., Wike, C.L., Weaver, B.D., Pflueger, C., Emery, B.R., Wilcox, A.L., et al. (2017). Conserved roles of mouse DUX and human DUX4 in activating cleavage-stage genes and MERVL/HERVL retrotransposons. Nat. Genet. *49*, 925–934. https://doi.org/10.1038/ng.3844.
15. Whiddon, J.L., Langford, A.T., Wong, C.J., Zhong, J.W., and Tapscott, S.J. (2017). Conservation and innovation in the DUX4-family gene network. Nat. Genet. *49*, 935–940. https://doi.org/10.1038/ng.3846.
16. De Iaco, A., Planet, E., Coluccio, A., Verp, S., Duc, J., and Trono, D. (2017). DUX-family transcription factors regulate zygotic genome activation in placental mammals. Nat. Genet. *49*, 941–945. https://doi.org/10.1038/ng.3858.
17. Chen, Z., and Zhang, Y. (2019). Loss of DUX causes minor defects in zygotic genome activation and is compatible with mouse development. Nat. Genet. *51*, 947–951. https://doi.org/10.1038/s41588-019-0418-7.
18. Bosnakovski, D., Gearhart, M.D., Ho Choi, S., and Kyba, M. (2021). Dux facilitates post-implantation development, but is not essential for zygotic genome activation. Biol. Reprod. *104*, 83–93. https://doi.org/10.1093/biolre/ioaa179.
19. De Iaco, A., Verp, S., Offner, S., Grun, D., and Trono, D. (2020). DUX is a non-essential synchronizer of zygotic genome activation. Development *147*, dev177725. https://doi.org/10.1242/dev.177725.
20. Chew, G.L., Campbell, A.E., De Neef, E., Sutliff, N.A., Shadle, S.C., Tapscott, S.J., and Bradley, R.K. (2019). DUX4 Suppresses MHC Class I to Promote Cancer Immune Evasion and Resistance to Checkpoint Blockade. Dev. Cell *50*, 658–671.e7. https://doi.org/10.1016/j.devcel.2019.06.011.
21. Preussner, J., Zhong, J., Sreenivasan, K., Günther, S., Engleitner, T., Künne, C., Glatzel, M., Rad, R., Looso, M., Braun, T., et al. (2018). Oncogenic Amplification of Zygotic Dux Factors in Regenerating p53-Deficient Muscle Stem Cells Defines a Molecular Cancer Subtype. Cell Stem Cell *23*, 794–805.e4. https://doi.org/10.1016/j.stem.2018.10.011.
22. Bosnakovski, D., Oyler, D., Mitanoska, A., Douglas, M., Ener, E.T., Shams, A.S., and Kyba, M. (2022). Persistent Fibroadipogenic Progenitor Expansion Following Transient DUX4 Expression Provokes a Profibrotic State in a Mouse Model for FSHD. Int. J. Mol. Sci. *23*, 1983. https://doi.org/10.3390/ijms23041983.
23. Jiang, S., Williams, K., Kong, X., Zeng, W., Nguyen, N.V., Ma, X., Tawil, R., Yokomori, K., and Mortazavi, A. (2020). Single-nucleus RNA-seq identifies divergent populations of FSHD2 myotube nuclei. PLoS Genet. *16*, e1008754. https://doi.org/10.1371/journal.pgen.1008754.
24. Lee, J.K., Bosnakovski, D., Toso, E.A., Dinh, T., Banerjee, S., Bohl, T.E., Shi, K., Orellana, K., Kyba, M., and Aihara, H. (2018). Crystal Structure of the Double Homeodomain of DUX4 in Complex with DNA. Cell Rep. *25*, 2955–2962.e3. https://doi.org/10.1016/j.celrep.2018.11.060.
25. Banerji, C.R.S., Panamarova, M., Hebaishi, H., White, R.B., Relaix, F., Severini, S., and Zammit, P.S. (2017). PAX7 target genes are globally repressed in facioscapulohumeral muscular dystrophy skeletal muscle. Nat. Commun. *8*, 2152. https://doi.org/10.1038/s41467-017-01200-4.
26. Banerji, C.R.S., and Zammit, P.S. (2019). PAX7 target gene repression is a superior FSHD biomarker than DUX4 target gene activation, associating with pathological severity and identifying FSHD at the single-cell level. Hum. Mol. Genet. *28*, 2224–2236. https://doi.org/10.1093/hmg/ddz043.
27. Bosnakovski, D., da Silva, M.T., Sunny, S.T., Ener, E.T., Toso, E.A., Yuan, C., Cui, Z., Walters, M.A., Jadhav, A., and Kyba, M. (2019). A novel P300 inhibitor reverses DUX4-mediated global histone H3 hyperacetylation, target gene expression, and cell death. Sci. Adv. *5*, eaaw7781. https://doi.org/10.1126/sciadv.aaw7781.
28. Bosnakovski, D., Ener, E.T., Cooper, M.S., Gearhart, M.D., Knights, K.A., Xu, N.C., Palumbo, C.A., Toso, E.A., Marsh, G.P., Maple, H.J., et al. (2021). Inactivation of the CIC-DUX4 oncogene through P300/CBP inhibition, a therapeutic approach for CIC-DUX4 sarcoma. Oncogenesis *10*, 68. https://doi.org/10.1038/s41389-021-00357-4.
29. Beerli, R.R., Segal, D.J., Dreier, B., and Barbas, C.F., 3rd (1998). Toward controlling gene expression at will: specific regulation of the erbB-2/HER-2 promoter by using polydactyl zinc finger proteins constructed from modular building blocks. Proc. Natl. Acad. Sci. USA *95*, 14628–14633. https://doi.org/10.1073/pnas.95.25.14628.
30. Yu, X., Liang, S., Chen, M., Yu, H., Li, R., Qu, Y., Kong, X., Guo, R., Zheng, R., Izsvák, Z., et al. (2022). Recapitulating early human development with 8C-like cells. Cell Rep. *39*, 110994. https://doi.org/10.1016/j.celrep.2022.110994.
31. Peaston, A.E., Evsikov, A.V., Graber, J.H., de Vries, W.N., Holbrook, A.E., Solter, D., and Knowles, B.B. (2004). Retrotransposons regulate host genes in mouse oocytes and preimplantation embryos. Dev. Cell *7*, 597–606. https://doi.org/10.1016/j.devcel.2004.09.004.
32. Eidahl, J.O., Giesige, C.R., Domire, J.S., Wallace, L.M., Fowler, A.M., Guckes, S.M., Garwick-Coppens, S.E., Labhart, P., and Harper, S.Q. (2016). Mouse Dux is myotoxic and shares partial functional homology with its human paralog DUX4. Hum. Mol. Genet. *25*, 4577–4589. https://doi.org/10.1093/hmg/ddw287.
33. Bosnakovski, D., Toso, E.A., Hartweck, L.M., Magli, A., Lee, H.A., Thompson, E.R., Dandapat, A., Perlingeiro, R.C.R., and Kyba, M. (2017). The DUX4 homeodomains mediate inhibition of myogenesis and are functionally exchangeable with the Pax7 homeodomain. J. Cell Sci. *130*, 3685–3697. https://doi.org/10.1242/jcs.205427.
34. Wong, C.J., Whiddon, J.L., Langford, A.T., Belleville, A.E., and Tapscott, S.J. (2022). Canine DUXC: implications for DUX4 retrotransposition and preclinical models of FSHD. Hum. Mol. Genet. *31*, 1694–1704. https://doi.org/10.1093/hmg/ddab352.
35. Bosnakovski, D., Daughters, R.S., Xu, Z., Slack, J.M.W., and Kyba, M. (2009). Biphasic myopathic phenotype of mouse DUX, an ORF within conserved FSHD-related repeats. PLoS One *4*, e7003. https://doi.org/10.1371/journal.pone.0007003.
36. Vega-Sendino, M., Olbrich, T., Stein, P., Tillo, D., Carey, G.I., Virginia, S., Saykali, B., Domingo, C.N., Maity, T.K., Jenkins, L.M., et al. (2022). The homeobox transcription factor DUXBL controls exit from totipotency. Preprint at bioRxiv. https://doi.org/10.1101/2022.09.19.508541v1.
37. Ganassi, M., Figeac, N., Reynaud, M., Ortuste Quiroga, H.P., and Zammit, P.S. (2022). Antagonism Between DUX4 and DUX4c Highlights a Pathomechanism Operating Through beta-Catenin in Facioscapulohumeral Muscular Dystrophy. Front. Cell Dev. Biol. *10*, 802573. https://doi.org/10.3389/fcell.2022.802573.
38. Zhu, C.H., Mouly, V., Cooper, R.N., Mamchaoui, K., Bigot, A., Shay, J.W., Di

Santo, J.P., Butler-Browne, G.S., and Wright, W.E. (2007). Cellular senescence in human myoblasts is overcome by human telomerase reverse transcriptase and cyclin-dependent kinase 4: consequences in aging muscle and therapeutic strategies for muscular dystrophies. Aging Cell *6*, 515–523. https://doi.org/10.1111/j.1474-9726.2007.00306.x.

39. Kendall, S.D., Linardic, C.M., Adam, S.J., and Counter, C.M. (2005). A network of genetic events sufficient to convert normal human cells to a tumorigenic state. Cancer Res. *65*, 9824–9828. https://doi.org/10.1158/0008-5472.CAN-05-1543.
40. Hayer, A., Shao, L., Chung, M., Joubert, L.M., Yang, H.W., Tsai, F.C., Bisaria, A., Betzig, E., and Meyer, T. (2016). Engulfed cadherin fingers are polarized junctional structures between collectively migrating endothelial cells. Nat. Cell Biol. *18*, 1311–1323. https://doi.org/10.1038/ncb3438.
41. Buenrostro, J.D., Wu, B., Chang, H.Y., and Greenleaf, W.J. (2015). ATAC-seq: A Method for Assaying Chromatin Accessibility Genome-Wide. Curr. Protoc. Mol. Biol. *109*, 21.29.1–21.29.9. https://doi.org/10.1002/0471142727.mb2129s109.
42. Bolger, A.M., Lohse, M., and Usadel, B. (2014). Trimmomatic: a flexible trimmer for Illumina sequence data. Bioinformatics *30*, 2114–2120.
43. Dobin, A., Davis, C.A., Schlesinger, F., Drenkow, J., Zaleski, C., Jha, S., Batut, P., Chaisson, M., and Gingeras, T.R. (2013). STAR: ultrafast universal RNA-seq aligner. Bioinformatics *29*, 15–21.
44. Alec Wysoker, McCowan, M., Homer, N., Fennell, T., and Picard. A set of tools (in Java) for working with next generation sequencing sata in the BAM format. http://broadinstitute.github.io/picard/.
45. Zhang, Y., Liu, T., Meyer, C.A., Eeckhoute, J., Johnson, D.S., Bernstein, B.E., Nusbaum, C., Myers, R.M., Brown, M., Li, W., and Liu, X.S. (2008). Model-based analysis of ChIP-Seq (MACS). Genome Biol. *9*, R137.
46. Love, M.I., Huber, W., and Anders, S. (2014). Moderated estimation of fold change and dispersion for RNA-seq data with DESeq2. Genome Biol. *15*, 550.
47. Kabsch, W. (2010). Xds. Acta Crystallogr. D Biol. Crystallogr. *66*, 125–132. https://doi.org/10.1107/S0907444909047337.
48. McCoy, A.J., Grosse-Kunstleve, R.W., Adams, P.D., Winn, M.D., Storoni, L.C., and Read, R.J. (2007). Phaser crystallographic software. J. Appl. Crystallogr. *40*, 658–674. https://doi.org/10.1107/S0021889807021206.
49. Emsley, P., Lohkamp, B., Scott, W.G., and Cowtan, K. (2010). Features and development of Coot. Acta Crystallogr. D Biol. Crystallogr. *66*, 486–501. https://doi.org/10.1107/S0907444910007493.
50. Adams, P.D., Afonine, P.V., Bunkóczi, G., Chen, V.B., Davis, I.W., Echols, N., Headd, J.J., Hung, L.W., Kapral, G.J., Grosse-Kunstleve, R.W., et al. (2010). PHENIX: a comprehensive Python-based system for macromolecular structure solution. Acta Crystallogr. D Biol. Crystallogr. *66*, 213–221. https://doi.org/10.1107/S0907444909052925.

STAR★METHODS

KEY RESOURCES TABLE

REAGENT or RESOURCE	SOURCE	IDENTIFIER
Antibodies		
GAPDH-HRP	Proteintech	60004; RRID: AB_2107436
rabbit anti-Histone H3K18Ac	Abcam	ab1191; RRID: AB_298692
rabbit anti-Histone H3K27Ac	Abcam	ab1791; RRID: AB_302613
anti-FLAG M2-Peroxidase	Sigma	A8592; RRID: AB_439702
HRP conjugated anti-rabbit	Jackson Immuno Research	111-035-003; RRID: AB_2313567
Bacterial and virus strains		
Stellar competent cells	Takara BIO INC.	Cat#636763
Chemicals, peptides, and recombinant proteins		
DMEM, high glucose	HyClone	Cat#SH30081.01
Ham's F10	Cytiva	Cat#SH30025.01
FBS	PEAK Serum	Cat#PS-FB3
Penicillin/streptomycin	Life Technologies	Cat#15140-122
Glutamax	Millipore	Cat#SCR006
Recombinant Human FGF basic	R&D Systems	Cat#233-FB-001MG/CF
2-Mercaptoethanol	Sigma	Cat#M3148-100ML
Dexamethasone	Cayman Chemical	Cat#11015
Insulin-Transferrin-Selenium-Sodium Pyruvate (ITS-A)	Gibco	Cat#51300-044
MEM Non-Essential Amino Acids Solution	Gibco	Cat#11140050
0.25% Trypsin-EDTA	Life Technologies	Cat#25200-072
PBS	HyClone	Cat#SH30256.01
Doxycycline	Alfa Aesar	Cat#J60579-14
Polybrene	Millipore	Cat#TR-1003-G
Puromycin	Invivogen	Cat#NC9138068
NheI-HF	New England BioLabs	Cat#R3131S
NotI-HF	New England BioLabs	Cat#R3189L
XhoI	New England BioLabs	Cat#R0146S
HindIII-HF	New England BioLabs	Cat#R3104M
Complete EDTA-free Protease Inhibitor Cocktail	Millipore	Cat#11873580001
Pierce ECL Western Blotting Substrate	Thermo Scientific	Cat#32106
Critical commercial assays		
CloneAmp HiFi PCR Premix	Takara BIO INC.	Cat#639298
In-Fusion HD Cloning Kit	Clontech	Cat#638909
TransIT-LTI transfection reagent	Mirus Bio LLC	Cat#MIR2300
Dual-Glo Luciferase Assay System	Promega	Cat#E2940
QIAPrep Spin MiniPrep Kit	Qiagen	Cat#27106
Quick-RNA Miniprep Kit	Zymo Research	Cat#R1055
Verso cDNA Synthesis Kit	Thermo	Cat#AB1453B
SYBR Premix Ex Taq	Takara BIO INC.	Cat#RR420A
Premix Ex Taq (Probe qPCR)	Takara BIO INC.	Cat#RR390B

(*Continued on next page*)

Continued

REAGENT or RESOURCE	SOURCE	IDENTIFIER
CellTiter-Glo Luminescent Cell Viability Assay	Promega	Cat#G7572
Click-iT Plus EdU Alexa Fluor 647 Flow Cytometry Assay Kit	Life Technologies	Cat#C10634
APC Annexin V Apoptosis Detection Kit with 7-AAD	BioLegend	Cat#640930
mMESSAGE mMACHINE T7 ULTRA Transcription Kit	Invitrogen	Cat#AM1345
TransIT-mRNA Transfection Kit	Mirus Bio LLC	Cat#MIR2225
Lipofectamine RNAiMAX Transfection Reagent	Invitrogen	Cat#13778030
Swift Rapid RNA Library Kit	Swift Biosciences	Cat#R2096
ON-TARGETplus Human DUXA (503835) siRNA - SMARTpool	Dharmacon	L-034920-02-0005
ON-TARGETplus Non-targeting siRNA #1	Dharmacon	D-001810-01-05
GAPDH Taqman Assay	Applied Biosystems	Hs99999905_m1
B2M Taqman Assay	Applied Biosystems	Hs00187842_m1
ZSCAN Taqman Assay	Applied Biosystems	Hs00357549_m1
LEUTX Taqman Assay	Applied Biosystems	Hs01028718_m1
PRAMEF1 Taqman Assay	Applied Biosystems	Hs04401269_sH
TRIM43 Taqman Assay	Applied Biosystems	Hs00299174_m1
MYH7 Taqman Assay	Applied Biosystems	Hs01110602_m1
DUX4 Taqman Assay	Applied Biosystems	Hs03037970_g1
MBD3L2 Taqman Assay	Applied Biosystems	Hs00544743_m1
Deposited data		
sDUX atomic coordinates, structure factors	Protein Data Bank	8EJO and 8EJP
ATAC-seq and ChIP-seq data	Gene Expression Omnibus	GSE214245 and GSE214230
Experimental models: Cell lines		
LHCN-M2	Vincent Mouly Lab	RRID: CVCL_8890
M007	This paper	N/A
M008	This paper	N/A
HEK293T	Michael Kyba Lab	N/A
HEK293T-iFLAG-DUX4	This paper	N/A
HEK293T-iFLAG-DUXA	This paper	N/A
HEK293T-iFLAG-DUXB	This paper	N/A
HEK293T-iFLAG-DUXA-VP64	This paper	N/A
HEK293T-iFLAG-DUXB-VP64	This paper	N/A
HEK293T-iFLAG-sDUX	This paper	N/A
HEK293T-iFLAG-sDUXΔC	This paper	N/A
LHCN-M2-iFLAG-DUX4	This paper	N/A
LHCN-M2-iFLAG-DUXA	This paper	N/A
LHCN-M2-iFLAG-DUXB	This paper	N/A
LHCN-M2-iFLAG-DUXA-VP64	This paper	N/A
LHCN-M2-iFLAG-DUXB-VP64	This paper	N/A
LHCN-M2-iFLAG-sDUX	This paper	N/A
M007-iDUXA	This paper	N/A

(*Continued on next page*)

Continued

REAGENT or RESOURCE	SOURCE	IDENTIFIER
M008-iDUXA	This paper	N/A
LHCN-M2iDUX4&DUXA	This paper	N/A
LHCN-M2iDUX4&GFP	This paper	N/A
Oligonucleotides		
DUXA	IDT	F: 5′ TCT TGC CCT GCT CTT CTT GT
DUXA	IDT	R: 5′ CCT GGG ATT GAT TCC AGA GA
DUXB	IDT	F: 5′ CCC TGA TAA AGC TGC CAG AG
DUXB	IDT	R: 5′ TGA GTC AGA TGC TGG GAC TG
RFPL4B	IDT	F: 5′ GGC TGA ATT CAA GTG GGT CT
RFPL4B	IDT	R: 5′ GAG ACG TAG GCT TCG GAT CTT
1X-TAATCA	IDT	AGCTACTCGAGTGACAGGGAGATCG TCTACAGCAGCGTAATCAACAGAAG CTTATCAG
1X-TAATCTAATCA	IDT	AGCTACTCGAGTGACAGGGAGATCG TCTACAGCAGCGTAATCTAATCAACA GAAGCTTATCAG
2X-TAATCTAATCA	IDT	AGCTACTCGAGGGATCCTTGACAGT AATCTAATCAACAGAGACAGTAATCT AATCAACAGGAGCTCAAGCTTATCA G
2X-TAATCTAATTA	IDT	GCTCGCTAGCCTCGAGGGATCCTTG ACAGTAATCTAATTAACAGAGACAGT AATCTAATTAACAGGAGCTCAAGCTT AGACACTAGA
2X-TGATTCAATCA	IDT	GCTCGCTAGCCTCGAGGGATCCTTG ACAGTGATTCAATCAACAGAGACAG TGATTCAATCAACAGGAGCTCAAGC TTAGACACTAGA
2X-TAATCAATTA	IDT	GCTCGCTAGCCTCGAGGGATCCTTG ACAGTAATCAATTAACAGAGACAGTA ATCAATTAACAGGAGCTCAAGCTTA GACACTAGA
2X-TAATCAATCA	IDT	GCTCGCTAGCCTCGAGGGATCCTTG ACAGTAATCAATCAACAGAGACAGT AATCAATCAACAGGAGCTCAAGCTT AGACACTAGA
2X-TAATTGATTA	IDT	AGCTACTCGAGTAATTGATTAGAGAT CAGTACTACAGCAGCGTAATTGATTA CAAGCTTATCAG
Recombinant DNA		
pSAM2-FLAG-DUX4	This paper	N/A
pSAM2-FLAG-DUXA	This paper	N/A
pSAM2-FLAG-DUXB	This paper	N/A
pSAM2-FLAG-DUXA-VP64	This paper	N/A
pSAM2-FLAG-DUXB-VP64	This paper	N/A
pSAM2-FLAG-sDUX	This paper	N/A
pSAM2-FLAG-sDUXΔC	This paper	N/A
pSAM-DUXA-ires-GFP	This paper	N/A
pGL4-1X-TAATCA	Michael Kyba Lab	N/A

(*Continued on next page*)

Continued

REAGENT or RESOURCE	SOURCE	IDENTIFIER
pGL4-1X-TAATCTAATCA	Michael Kyba Lab	N/A
pGL4-2X-TAATCTAATCA	Michael Kyba Lab	N/A
pGL4-2X-TAATCTAATTA	Michael Kyba Lab	N/A
pGL4-2X-TGATTCAATCA	Michael Kyba Lab	N/A
pGL4-2X-TAATCAATTA	Michael Kyba Lab	N/A
pGL4-2X-TAATCAATCA	Michael Kyba Lab	N/A
pGL4-2X-TAATTGATTA	Michael Kyba Lab	N/A
Software and algorithms		
Prism	GraphPad Software	https://www.graphpad.com/scientific-software/prism/
FlowJo	Becton Dickinson	https://www.flowjo.com/
Image Lab	Bio-Rad	https://www.bio-rad.com/en-us/product/image-labsoftware?ID=KRE6P5E8Z
ZEN Pro	Zeiss	https://www.zeiss.com/microscopy/en/products/software/zeiss-zen.html
R 4.2.1	R-Cran	https://cran.r-project.org/
DESeq	Bioconductor	https://www.bioconductor.org
ggplot2	Rstudio	https://www.tidyverse.org
Custom R scripts	This paper	https://github.com/micahgearhart/sDUXDUXABC.git

RESOURCE AVAILABILITY

Lead contact

Further information and requests for resources and reagents should be directed to and will be fulfilled by the lead contact, Michael Kyba (kyba@umn.edu).

Materials availability

Plasmids and cell lines generated by this study are available by request from the lead contact.

Data and code availability

- Atomic coordinates and structure factors have been deposited in the Protein DataBank (PDB) under accession codes 8EJO and 8EJP. RNA-seq, ATAC-seq, and ChIP-seq data have been submitted to GEO (GSE214245 and GSE214230).
- Scripts used are available at https://github.com/micahgearhart/sDUX-DUXABC.git.
- Any additional information required to reanalyze the data reported in this paper is available from the lead contact upon request.

EXPERIMENTAL MODEL AND STUDY PARTICIPANT DETAILS

Four immortalized human cell lines were used to derive cell lines this study:

- LHCN-M2 immortalized human myoblasts,[38] genotype: WT; sex: male; race: unknown; authentication: tested for differentiation.
- HEK293T cells; genotype/sex/race: unknown; authentication: human sequence only.
- M007 immortalized human myoblasts (this study); genotype: WT; sex: female; race: Caucasian; authentication: established in this study, tested for differentiation.
- M008 immortalized human myoblasts (this study); genotype: FSHD; sex: male; race: Caucasian; authentication: established in this study, tested for differentiation.

Cell lines were not routinely tested for mycoplasma contamination.
Human subjects work was performed in accordance with a protocol approved by the University of Minnesota IRB.

METHOD DETAILS

Synthesis of expression constructs

The full length coding sequence for sDUX was identified by running the TBLASTN algorithm with the single platypus homeodomain sequence identified by Leidenroth and Hewitt against the platypus (mOrnAna1.p.v1) genome. The top hit (E-value = 5e-23) was found in the gene ENSOANG00000047618 located at chr3:113694167-113694310 adjacent to TMEM254 (CJ057) and ANXA11. A codon optimized version of the ENSOANG00000047618 open reading frame was synthesized by Biomatik. cDNAs for DUXA and DUXB were synthesized by Integrated DNA Technologies. FLAG and VP64 sequences were added by PCR amplification, and fragments were cloned into the pSAM2-Puro lentiviral vector[13] by In-Fusion HD Cloning (Takara).

Cell culture

Control LHCN-M2 immortalized human myoblasts[38] and FSHD (M008) immortalized human myoblasts were cultured in F10 medium (HyClone) with 20% FBS (Peak Serum), 2-mercaptoethanol 1x (Gibco), 10^{-9} M dexamethasone (Sigma), 10 ng/mL bFGF (Peprotech), Glutamax (Gibco), and Penicillin/Streptomycin (P/S, Gibco) at 37°C and 5% CO_2. Immortalized M008 cells were derived by transducing primary myoblasts obtained from CD56 sorting of mononuclear cells from a muscle biopsy of an individual with FSHD under a protocol approved by the University of Minnesota IRB, with pbabe-cyclinD1+CDK4R24C (gift of Christopher Counter, Addgene)[39] and pLV-hTERT-IRES-hygro (gift of Tobias Meyer, Addgene).[40] The M007iDUX4 and M008iDUXA cell lines were generated from M007 and M008 immortalized myoblasts, which were derived by transduction of primary myoblasts from control and FSHD donors respectively, with two lentivectors, FUGW-rtTA and pSAM2-DUXA as previously described.[13] The LHCN-M2iDUX4&DUXA cell line was generated by transducing LHCN-M2iDUX4 cells with pSAM-DUXA-ires-GFP lentivirus. GFP positive cells were FACS sorted two days post infection using a BD FACSAria (BD Biosciences, Franklin Lakes, NJ).

Myogenic differentiation was performed on gelatin (0.1%) coated dishes. Confluent cultures were washed once with PBS without Ca^{2+}/Mg^{2+}, and fed with differentiation medium (DMEM/F12 (Corning Cellgro) with 1x insulin/transferrin/selenium (Gibco), 1x NEAA (Gibco), Glutamax and P/S.

RNA interference

Cells were seeded into 24-well plates (1.5× 10^5/well), and the following day 50 nM siRNA for DUXA (L-034920-02-0005) or non-targeted control (D-001810-01-05) (SMARTpool, Dharmacon) were transfected using Lipofectamine RNAiMAX (Invitrogen). RNA was isolated 48 hours post-transfection and the effect on cell viability was analyzed at 72 and 96 hours post-transfection.

EdU incorporation

EdU incorporation was measured using a Click-iT Plus EdU Flow Cytometry Assay Kit (Invitrogen). Cells were fixed and permeabilized in suspension, then incubated in Click-iT Plus reaction cocktail containing Alexa Fluor 647 picolyl azide. Flow cytometry was performed on a BD FACS Aria (BD Biosciences).

Annexin V/7-AAD staining

Cells were trypsinized and stained with Annexin V and 7-AAD using APC Annexin V staining kit (BioLegend) according to the manufacturer's instructions. Stained cells were evaluated on a FACSAria II (BD) and analyzed using FlowJo (FlowJo, LLC).

Transduction

Viral supernatants were produced in 293T cells by transfection of lentivector DNA together with pVSVG and Δ8.9 packaging constructs, using Mirus TransIT-LTI transfection reagent (Mirus Bio). Medium was changed after 24 hours, and the viral supernatants were collected 48 hours post-transfection. Supernatants were then syringe-filtered (0.45 μm) and supplemented with 10 μg/mL polybrene (Millipore Sigma). Cells were incubated in viral supernatant diluted 1:2 overnight at 37°C, after which the supernatant was replaced with fresh culture medium. Infected cells were selected by Puromycin treatment (2.0 μg/mL) for 3 days.

Cell viability (ATP) assay

Cells were plated in a 96 well dish (1 × 10^5 cells/well), and the following day were induced with doxycycline. ATP assays were performed using CellTiter-Glo Luminescent Cell Viability Assay (Promega) according to the manufacturer's instructions. Luminescence was analyzed on POLARstar Optima Microplate Reader (BMG Labtech, Offenburg, Germany).

Dual Glo luciferase assay

Cells were plated in a 96 well dish (1 × 10^5 cells/well), and transfected the following day with both the Renilla Luc control reporter (CMV-Renilla) and various Firefly Luc reporter constructs, containing different versions of the homeodomain binding motif, using Mirus TransIT-LTI transfection reagent (Mirus Bio). The following day, cells were induced with either 500 or 1,000 ng/ml doxycycline. After 24 hrs, luciferase

levels were quantified using the Dual-Glo Luciferase Assay System (Promega) according to the manufacturer's instructions. Luminescence was measured using the Cytation3 plate reader (BioTek).

mRNA generation and transfection

Synthetic mRNAs were generated using mMESSAGE mMACHINE T7 ULTRA Transcription Kit (Invitrogen) using PCR product templates, which were produced by incorporating a T7 promoter sequence into the forward primers. Following ARCA-capped transcription and poly(A) tailing, synthetic RNA was purified and recovered using a QuickRNA miniprep kit (Zymo Research). Transfection of cells with mRNAs was achieved using a TransIT-mRNA transfection kit (Mirus Bio) according to the manufacturer's instructions.

Western blots

Cells were lysed with RIPA buffer supplemented with protease inhibitor cocktail (Complete, Roche), and proteins were separated on 10% SDS-PAGE gels, then transferred to PVDF membranes. Antibodies were diluted in 5% skim milk in TBST and incubated overnight at 4°C or 1 hour at RT. An appropriate HRP conjugated secondary antibody was incubated for 1 hour at RT. Membranes were then washed with TBST, and signal was visualized using Pierce ECL western blotting substrate (Thermo Scientific). Antibodies used in the study: GAPDH-HRP (1:5000, 60004, Proteintech), rabbit anti-Histone H3K18Ac (1:500, ab1191, Abcam), rabbit anti-Histone H3K27Ac (1:500, ab1791, Abcam, lot: GR3297878-1), anti-FLAG M2-Peroxidase (HRP, 1:10000, A8592, Sigma), and HRP conjugated anti-rabbit (1:5000, 111-035-003, Jackson Immuno Research, lot: 149393).

RNA isolation, quantitative real time RT-PCR (RTqPCR) and RNAseq

RNA was extracted using the Zymo RNA extraction kit following the manufacture's protocol. cDNA was made using 0.5 μg total RNA with oligo-dT primer and Verso cDNA Synthesis Kit (Thermo Scientific) following the manufacturer's instructions. qPCR was performed by using Premix Probe Ex Taq or SYBR-green (Takara) and commercially available probes from Applied Biosystems (*GAPDH*, Hs99999905_m1; *B2M*, Hs00187842_m1; *ZSCAN*, Hs00357549_m1; *LEUTX*, Hs01028718_m1; *PRAMEF1*, Hs04401269, *TRIM43*, Hs00299174_m1, *MYH7*, Hs01110602_m1, *DUX4*, Hs03037970_g1, *MBD3L2*, Hs00544743_m1) or custom-designed primers (*DUXA*: F: 5′ TCT TGC CCT GCT CTT CTT GT and R: 5′ CCT GGG ATT GAT TCC AGA GA; *DUXB* F: 5′ CCC TGA TAA AGC TGC CAG AG and R: 5′ TGA GTC AGA TGC TGG GAC TG; *RFPL4B* F: 5′ GGC TGA ATT CAA GTG GGT CT and R: 5′ GAG ACG TAG GCT TCG GAT CTT). Gene expression levels were normalized to that of *GAPDH* or *B2M* and analyzed with 7500 System Software using the ΔCT method (Applied Biosystems).

RNA-seq library preparation was done with 500 ng total RNA. One set of libraries (Figure 3) was prepared using the Swift Rapid RNA Library Kit (SwiftBioscience) and 36 base paired-end sequenced on an Illumina NextSeq at the University of Minnesota Genomics Center (UMGC). The other set (Figure 4) was prepared and sequenced (2 × 150 paired-end) on an Illumina HiSeq at Genewiz (NJ, USA). Conventional gene expression was quantified using Salmon (v1.9) with the human Gencode v38 transcriptome modified to contain the sDUX coding sequence. Analysis of expression of repetitive elements was performed by mapping trimmed reads to the GRCh38 genome with Star (v2.7.2) and enumerating the reads mapping to UCSC RMSK features using Rsubread allowing for fractional counts. Gene expression differences for conventional genes and repetitive elements was performed with DESeq2 (v1.36.0).

ATAC-seq

For each construct, biological duplicates from doxycycline-treated and untreated myoblasts were collected using Trypsin-EDTA followed by dilution with culture medium and centrifugation at 400g for 5 minutes. 50,000 cells were washed with 200 μL of cold PBS then resuspended in 100 μL of cold lysis buffer (10mM Tris-HCl pH 7.4, 10mM NaCl, 3mM MgCl2, 0.1% IGEPAL CA-630), spun at 500 g for 10 minutes at 4°C and resuspended in 50 μL of the transposition reaction mix. Transposition occurred at 37°C for 30 minutes, after which transposed DNA was purified using a Qiagen MinElute Kit and eluted in 10μL Elution Buffer. Chromatin accessibility studies were performed following the protocol described by.[41] PCR amplification using Illumina-compatible adapter-barcodes and final library preparation were performed at the UMGC. After Quality Control, libraries were pooled and sequenced on NovaSeq S4 2x150-bp run (Illumina). Mapping to the human hg38 genome and peak calling were performed using the ENCODE ATAC-seq pipeline.

ChIP-seq sample and library preparation

HEK293 cells were transfected with Doxycycline inducible plasmids either encoding for V5 epitope-tagged DUX4 or DUXA. 24 h after later, gene expression was induced by addition of Doxycycline (Sigma, D9891-10G) to a final concentration of 100 ng/ml for 24 h. Next, chromatin-protein complexes were cross-linked by addition of methanol-free formaldehyde (ThermoFisher, 28906) at a final concentration of 1 % for 10 min at RT. Cells were then washed three times in PBS and chromatin was isolated and sheared to 200-700 bp using the truChIP Chromatin Shearing Kit (Covaris, 520154) and a Covaris E220evolution focused-ultrasonicator following the manufacturer's recommendations. Subsequently, 30 μg of chromatin was diluted 1:4 with RIPA-buffer (10 mM Tris-HCl pH 8.0, 1 mM EDTA pH 8.0, 140 mM NaCl, 1 % Triton X-100, 0.1 % sodium deoxycholate) and incubated with 4 μg anti-V5-antibody (Abcam, ab9116) at 4°C overnight. Antibody-bound chromatin was then coupled to protein A beads (Diagenode, C03020002) for three hours at 4°C. Samples were then washed four times with RIPA-buffer, two times with high-salt-RIPA-buffer (10 mM Tris-HCl pH 8.0, 1 mM EDTA pH 8.0, 500 mM NaCl, 1 % Triton X-100, 0.1 % sodium deoxycholate), two times with LiCl-buffer (10 mM Tris-HCl pH 8.0, 1 mM EDTA pH 8.0, 250 mM LiCl, 0.5 % NP-40, 0.5 % sodium deoxycholate) and finally two

times with TE Buffer (10 mM Tris-HCl pH 8.0, 1 mM EDTA pH 8.0). RNA was eliminated by addition of RNAseA (Thermo Fisher Scientific, EN0531) to a final concentration of 0.1 mg/ml in 10 mM Tris-HCl pH 8.0, 1 mM EDTA pH 8.0, 300 mM NaCl, 0.5 % SDS and incubated at 37°C for 30 min. Reverse crosslinking was achieved by addition of Proteinase K (ThermoFisher, EO0491) to a final concentration of 0.4 mg/ml and incubation at 55°C for 1 h and then at 65°C overnight. DNA was purified using the NucleoSpin Gel and PCR Clean-up kit (Macherey-Nagel, 740609) and quantified by Qubit dsDNA HS Assay Kit (Thermo Fisher Scientific). 2-3 ng of DNA was used as input for TruSeq ChIP Library Preparation Kit (Illumina) with following modifications. Instead of gel-based size selection before final PCR step, libraries were size selected by SPRI-bead based approach after final PCR with 18 cycles. In detail, samples were 1st cleaned up by 1x bead:DNA ratio to eliminate residuals from PCR reaction, followed by 2-sided-bead cleanup step with initially 0.6x bead:DNA ratio to exclude larger fragments. Supernatant was transferred to new tube and incubated with additional beads in 0.2x bead:DNA ratio for eliminating smaller fragments, like adapter and primer dimers. Bound DNA samples were washed with 80% ethanol, dried and resupended in TE buffer. Library integrity was verified with LabChip Gx Touch 24 (Perkin Elmer). Sequencing was performed on the NextSeq500 instrument (Illumina) using v2 chemistry with 1x75bp single end setup.

ChIP-seq analysis

Trimmomatic version 0.39 was employed to trim reads after a quality drop below a mean of Q20 in a window of 20 nucleotides and keeping only filtered reads longer than 15 nucleotides (Bolger et al.,[42] Trimmomatic: a flexible trimmer for Illumina sequence data). Reads were aligned versus Ensembl human genome version hg38 (Ensembl release 104) with STAR 2.7.10a (Dobin et al.,[43] STAR: ultrafast universal RNA-seq aligner). Aligned reads were filtered to remove: duplicates with Picard 2.27.1[44] (Picard: A set of tools (in Java) for working with next generation sequencing data in the BAM format), spliced, multi-mapping, ribosomal, or mitochondrial reads. Peak calling was performed with Macs version 3.0.0a6 with FDR < 0.1 and "–scale-to large" (Zhang et al.,[45] Model-based Analysis of ChIP-Seq). Peaks overlapping ENCODE blacklisted regions (known misassemblies, satellite repeats) were excluded. Remaining peaks were unified to represent a common set of regions for all samples and counts were produced with bigWigAverageOverBed (UCSC Toolkit). The raw count matrix was normalized with DESeq2 version 1.30.1 (Love et al.,[46] Moderated estimation of fold change and dispersion for RNA-Seq data with DESeq2). Peaks were annotated with the gene + promoter (TSS +- 5000 nt) with the largest overlap based on Ensembl release 104. Contrasts were created with DESeq2 based on the normalized union peak matrix with size factors set to zero. Peaks were classified as significantly differential at average count > 10 and -1 < log2FC > 1.

Immunofluorescence

Cells were fixed in 4% PFA for 10 min., washed twice with PBS, permeabilized with 0.3% Triton X for 30 min, and blocked with 3% BSA for 1 hour at RT. Primary antibody (MF20, 1:20, Hybridoma bank, University of Iowa) was diluted in 3% BSA and incubated ON at 4°C. Secondary antibody (Alexa fluor 555 Goat Anti-Mouse, 1:500, Invitrogen) was applied for 60 min at RT. Nuclei were visualized using DAPI (1:5000, Sigma).

Biochemical and structural studies

The homeodomain of platypus sDUX was expressed as MBP-fusion from a codon-optimized gene cloned into the pMAL-c5x bacterial expression vector. The construct contained an 8xHis-tag and the Human Rhinovirus (HRV) 3C Protease cleavage site between MBP and sDUX. The protein was expressed in the *E. coli* strain BL21(DE3) and purified from the soluble bacterial extract using Ni-NTA affinity chromatography. After a treatment with HRV 3C protease, sDUX was further purified over a Superdex 75 size-exclusion column operating with 20 mM Tris-HCl, pH 7.4, 0.5 M NaCl, 5 mM β-mercaptoethanol, concentrated by ultrafiltration, flash-frozen in liquid nitrogen and stored at –80°C. The protein concentration was determined based on UV absorbance. The amino acid sequence of the purified sDUX HD was: GPAREGARRK RTTFNKTQLE ILVKSFNKDP YPGIGVREHL ASLIQIPESR IQVWFQNRRA RQLGQKKKLEV. DUX4 HD1-HD2 was prepared and EMSA conducted as described previously.[24]

For crystallographic studies, sDUX-DNA complex was prepared by mixing the purified protein with a 17 bp dsDNA substrate (5′-GCG TAA TCT AAT CAA CA-3′ / 5′-TGT TGA TTA GAT TAC GC-3′) at a molar ratio of 2:1 in 10 mM Tris-HCl, pH 7.4, 0.1 M NaCl, at a protein concentration of 20 mg ml^{-1}. The complex was crystallized in sitting drop vapor diffusion mode using the reservoir solution consisting of 0.2 M calcium chloride, 50 mM HEPES buffer, pH 7.5, 28% polyethylene glycol 400, 2 mM spermine. The sDUX-DNA crystals were cryo-protected by brief soaking in the reservoir solution supplemented with 20 % ethylene glycol and flash cooled by plunging in liquid nitrogen. X-ray diffraction data were collected at the NE-CAT beamline 24-ID-C of the Advanced Photon Source (Lemont, IL) and processed using XDS.[47] The structures were determined by molecular replacement with PHASER[48] using the DUX4-DNA complex (PDB ID: 6E8C)[24] as the search model. Iterative model building and refinement were conducted using COOT[49] and PHENIX.[50] To determine the identity of DNA strands in the pseudo-symmetrical complex, we collected additional data set on a crystal grown with the bottom strand containing a 5-bromouracil substitution (5′-TG/i5Br-dU/TGA TTA GAT TAC GC-3′), which gave an improved resolution albeit with strong anisotropy. A summary of crystallographic data statistics is shown in Table S1. Figures were generated using PyMOL (https://pymol.org/2/).

QUANTIFICATION AND STATISTICAL ANALYSIS

All experiments were repeated in at least in three biological replicates. Significance was calculated by one- or two-way ANOVA with GraphPad; **** indicates p<0.0001, *** p<0.001, ** p<0.01, and * p<0.05. Statistical details; including sample size and definition, center and dispersion and precision measures; may be found in the figure legends.